

Solar wind control of magnetospheric energy content: substorm quenching and multiple onsets

Article

Published Version

Karlsson, S. B. P., Opgenoorth, H. J., Eglitis, P., Kauristie, K., Syrjäso, M., Pulkkinen, T., Lockwood, M., Nakamura, R., Reeves, G. and Romanov, S. (2000) Solar wind control of magnetospheric energy content: substorm quenching and multiple onsets. *Journal of Geophysical Research*, 105 (A3). pp. 5335-5356. ISSN 0148-0227 doi: <https://doi.org/10.1029/1999JA900297> Available at <https://centaur.reading.ac.uk/38732/>

It is advisable to refer to the publisher's version if you intend to cite from the work. See [Guidance on citing](#).

Published version at: <http://dx.doi.org/10.1029/1999JA900297>

To link to this article DOI: <http://dx.doi.org/10.1029/1999JA900297>

Publisher: American Geophysical Union

All outputs in CentAUR are protected by Intellectual Property Rights law, including copyright law. Copyright and IPR is retained by the creators or other copyright holders. Terms and conditions for use of this material are defined in the [End User Agreement](#).

www.reading.ac.uk/centaur

CentAUR

Central Archive at the University of Reading

Reading's research outputs online

Solar wind control of magnetospheric energy content: Substorm quenching and multiple onsets

S. B. P. Karlsson,¹ H. J. Opgenoorth,^{1,2} P. Eglitis,^{1,2} K. Kauristie,²
M. Syrjäso, ² T. Pulkkinen,² M. Lockwood,³ R. Nakamura^{4,5}
G. Reeves,⁶ and S. Romanov ⁷

Abstract. In this paper we report coordinated multispacecraft and ground-based observations of a double substorm onset close to Scandinavia on November 17, 1996. The Wind and the Geotail spacecraft, which were located in the solar wind and the subsolar magnetosheath, respectively, recorded two periods of southward directed interplanetary magnetic field (IMF). These periods were separated by a short northward IMF excursion associated with a solar wind pressure pulse, which compressed the magnetosphere to such a degree that Geotail for a short period was located outside the bow shock. The first period of southward IMF initiated a substorm growth phase, which was clearly detected by an array of ground-based instrumentation and by Interball in the northern tail lobe. A first substorm onset occurred in close relation to the solar wind pressure pulse impinging on the magnetopause and almost simultaneously with the northward turning of the IMF. However, this substorm did not fully develop. In clear association with the expansion of the magnetosphere at the end of the pressure pulse, the auroral expansion was stopped, and the northern sky cleared. We will present evidence that the change in the solar wind dynamic pressure actively quenched the energy available for any further substorm expansion. Directly after this period, the magnetometer network detected signatures of a renewed substorm growth phase, which was initiated by the second southward turning of the IMF and which finally lead to a second, and this time complete, substorm intensification. We have used our multipoint observations in order to understand the solar wind control of the substorm onset and substorm quenching. The relative timings between the observations on the various satellites and on the ground were used to infer a possible causal relationship between the solar wind pressure variations and consequent substorm development. Furthermore, using a relatively simple algorithm to model the tail lobe field and the total tail flux, we show that there indeed exists a close relationship between the relaxation of a solar wind pressure pulse, the reduction of the tail lobe field, and the quenching of the initial substorm.

1. Introduction

The solar wind is the main source for the energy of the magnetosphere. It is today generally recognized that

the Z component of the interplanetary magnetic field (IMF), to a large extent, controls the energy input to the magnetosphere. As the IMF turns southward, the rate of reconnection at the subsolar magnetopause is enhanced, leading to an increase of open magnetic flux in the magnetosphere. This corresponds to more effective coupling of the magnetosphere to the solar wind dynamo and an increase in the magnetospheric electric field, driving a more intense convection. Increase in the lobe flux due to dayside magnetic field erosion leads to the development of a more tail-like magnetosphere, which involves an increase of the cross-tail current flowing in the neutral sheet between the tail lobes [McPherron, 1991].

After a certain loading period the so-called growth phase [McPherron, 1970, 1972; McPherron *et al.*, 1973], the magnetosphere reaches an unstable energy state, and the impulsive sporadic release of excess energy is possible and, indeed, very probable (the only exceptions are the so-called enhanced steady convection events

¹ Swedish Institute of Space Physics, Uppsala Division, Uppsala.

² Finnish Meteorological Institute, Helsinki.

³ Rutherford Appleton Laboratory, Chilton, Didcot, Oxfordshire, England, United Kingdom.

⁴ Solar Terrestrial Environment Laboratory, Nagoya University, Toyokawa, Japan.

⁵ Max-Planck-Institut für Extraterrestrische Physik, Garching, Germany.

⁶ Los Alamos National Laboratory, Los Alamos, New Mexico.

⁷ Space Research Institute, Russian Academy of Sciences, Moscow.

Copyright 2000 by the American Geophysical Union.

Paper number 1999JA900297.
0148-0227/00/1999JA900297\$09.00

[Sergeev *et al.*, 1996]). Even if substorm onset can occur completely untriggered and spontaneously, there is much discussion about possible trigger processes in the solar wind, the magnetosphere, or the ionosphere [Kan, 1993; Rostoker, 1983, 1996; Lyons, 1995, 1996; Caan *et al.*, 1973; Petrinec and Russell, 1996]. The various substorm theories mostly differ in their choice of the initial instability as the cause of the substorm, and therefore they often divert also in their different treatment of the question of substorm triggers.

In the Near-Earth Neutral Line (NENL) model [Baker *et al.*, 1984, 1985, 1996; Russell and McPherron, 1973; Hones *et al.*, 1987], the substorm sequence begins when a southward turning of the IMF activates day-side reconnection. Magnetic flux is transported back to the tail where a part of it is reconnected and convected back to the dayside magnetosphere. The remaining part of the field lines become added to the tail lobes, increasing the magnetic flux density and, owing to Biot-Savart's law, also increasing the neutral sheet current, stretching the field lines in the magnetotail. After a while (typically 1 hour), these field lines are suddenly reconnected in the tail, and their magnetic energy is explosively released. At about 20-30 R_E a new neutral line is formed, the Near-Earth Neutral Line, and the stretched field lines become dipolar. The large region between this and the distant neutral line then forms a magnetic plasmoid, which is finally ejected from the magnetosphere as the tailward retreating NENL starts to reconnect open magnetic flux.

In the Current Disruption (CD) model [Lui, 1991; Lui *et al.*, 1992; Lopez and Lui, 1990; Lopez *et al.*, 1988], a thin current sheet in the inner magnetosphere is formed owing to the same reasons as those in the NENL model. When the current sheet is sufficiently thin, an anomalous resistivity is built up in the plasma sheet that disrupts the current sheet. Because of the high inductance of the tail circuit, the current must continue to flow. This is accomplished by current diversion along the field lines to the ionosphere, forming the substorm current wedge. The current disruption begins close to geosynchronous orbit and expands radially outward [Lopez and Lui, 1990]. The model does not necessarily include any reconnection of open field lines in the tail lobe during the substorm expansion phase. It has instead been suggested that the disruption of the current sheet launches rarefaction waves down the tail which induces plasma sheet thinning and reduction of the vertical component of the magnetic field. At some point along the tail, probably during the late expansion phase or early recovery phase, these two effects give rise to reconnection and the formation of a plasmoid [Lui, 1991].

The magnetosphere-ionosphere coupling (MIC) model [Kan, 1993] concentrates on the effects that changes in the ionospheric conductivity can have on the magnetospheric sources of the field-aligned currents. Another type of magnetosphere-ionosphere coupling model considers the influence of heavy ionospheric ions, transport-

ed during the growth phase toward the inner near-Earth plasma sheet, and how this can give rise to current disruption [Baker *et al.*, 1982; Daglis *et al.*, 1994; Daglis and Axford, 1996]. Finally, there exist even other substorm models which place the origin of ionospheric auroral zone substorm expansion features into the plasma sheet boundary layer [Eastman *et al.*, 1985, 1988].

The main problem with all the various substorm models and theories is that they concentrate on explaining the onset of energy release only, mainly because the features of the later expansion phase and recovery phase are so complicated. Often the observed features are even mixed with the next substorm's growth phase and/or multiple substorm expansions. Depending on the priority of the authors of the various theories, more or less of the observed onset features are explained in detail; for example the CD model puts emphasis on the ground-based and near-Earth features, and the NENL model puts emphasis on the medium tail observations. A recent conjecture reached at the First International Conference on Substorms (ICS-1 in Kiruna, Sweden) [Kennel, 1992] has led to some more refined views, where several causal chains are considered possible; that is, CD can lead to NENL (as earlier proposed by Lui [1991]) or vice versa [Hesse and Birn, 1991a, b].

As the debate concerning substorm onset models was not progressing very much, several scientists began to concentrate on observational tests of the substorm theories, using data from the late expansion and recovery phase. Pellinen *et al.* [1992] and Opgenoorth *et al.* [1994] discussed the physical processes during the cessation of substorms in the substorm recovery phase. Several new features, basically supporting the NENL model, were resolved, but no final conclusions were reached. Other attempts to approach alternative aspects of the substorm sequence but not the onset itself were the studies of incomplete substorms, i.e. pseudo breakups [Koskinen *et al.*, 1992; Rostoker, 1998] or multiple onsets [Yeoman *et al.*, 1994]. Such studies involving signatures of more complicated patterns of substorm development lead in the end to the first attempt of a more modular approach to substorm modeling by Elphinstone *et al.* [1996].

In this paper we try to illustrate the possible solar wind control not of substorm onset but of substorm cessation. We will present observations from several satellites and a network of ground-based instrumentation (including the European Incoherent Scatter facility (EISCAT)) which can readily be explained with a solar wind controlled cancelation or "quenching of an almost fully developed substorm expansion. Such data allow for a critical discussion of the various substorm models (or theories), since the possibility for substorm inhibition, or "quenching, as we would like to call it, is not contained in all proposed mechanisms. From our data it appears that not only the cessation but even the onset of the observed substorm expansion could have been triggered by a solar wind pressure pulse after a period of

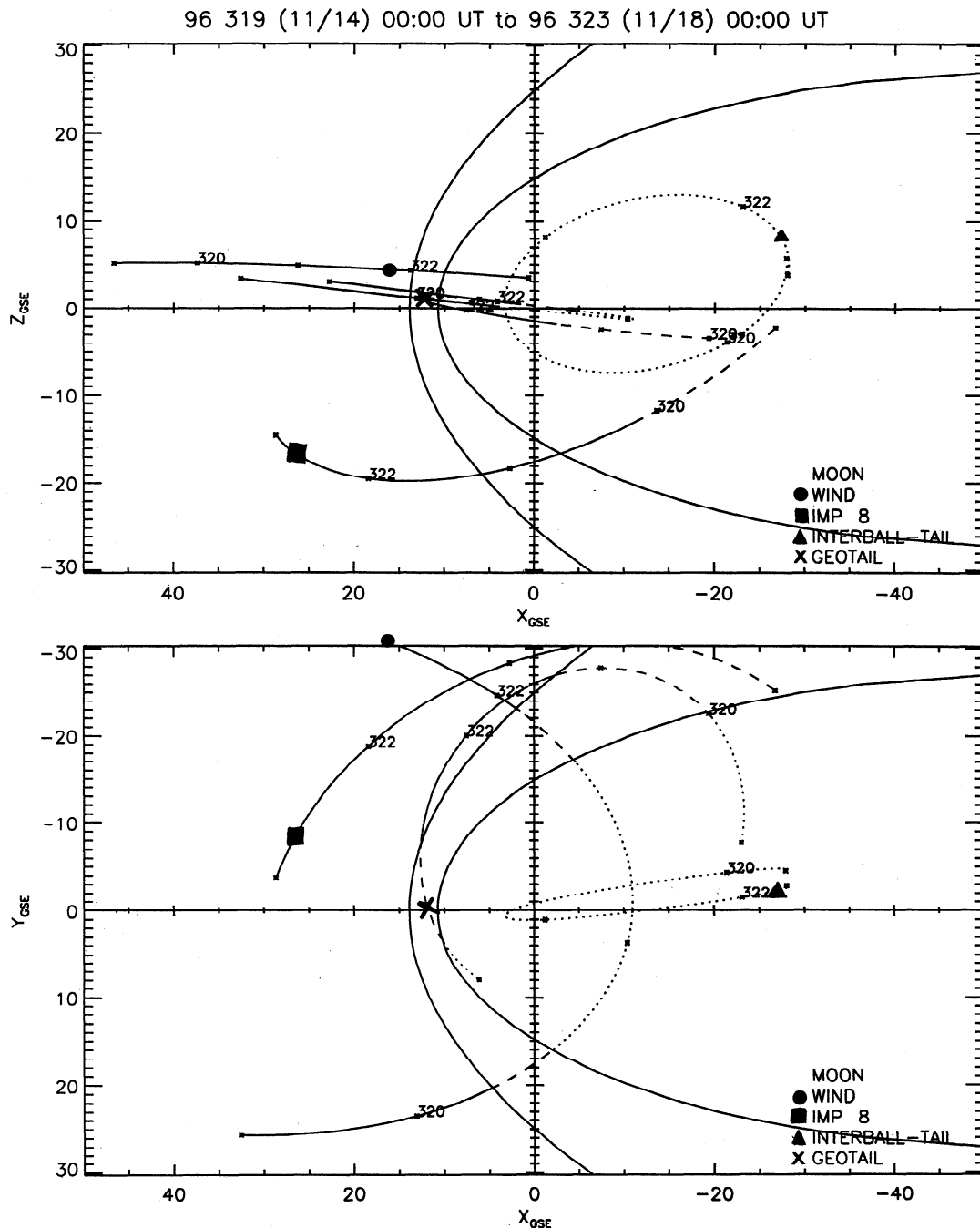


Figure 1. Partial orbital plots in the GSE $X-Z$ and $X-Y$ planes for key International Solar Terrestrial Physics (ISTP) programme satellites around November 17, 1996. The locations of Wind, IMP 8, Interball, and Geotail are marked according to the legend shown.

southward IMF. A second substorm growth phase and, as far as we can see, a purely spontaneous onset occur only 30 min after the first incomplete substorm event. This second substorm develops fully and ends with a typical substorm recovery phase.

2. Observations

The evening of November 17, 1996, was selected for specially coordinated ground-based experiments owing

to a favorable constellation of several satellites in the International Solar Terrestrial Physics (ISTP) programme. Figure 1, provided via the World Wide Web ISTP pages (M. Peredo et al., ISTP Spacecraft Orbit Plots at <http://www-spf.gsfc.nasa.gov/orbits/>), illustrates the positions of the Wind, IMP 8, Geotail, and Interball satellites during this event. It can be seen that two satellites, Wind and IMP 8, monitored the solar wind at $X=19 R_E$ and $X=26 R_E$, respectively. Geotail was in the magnetosheath at $X=11 R_E$, i.e., just outside

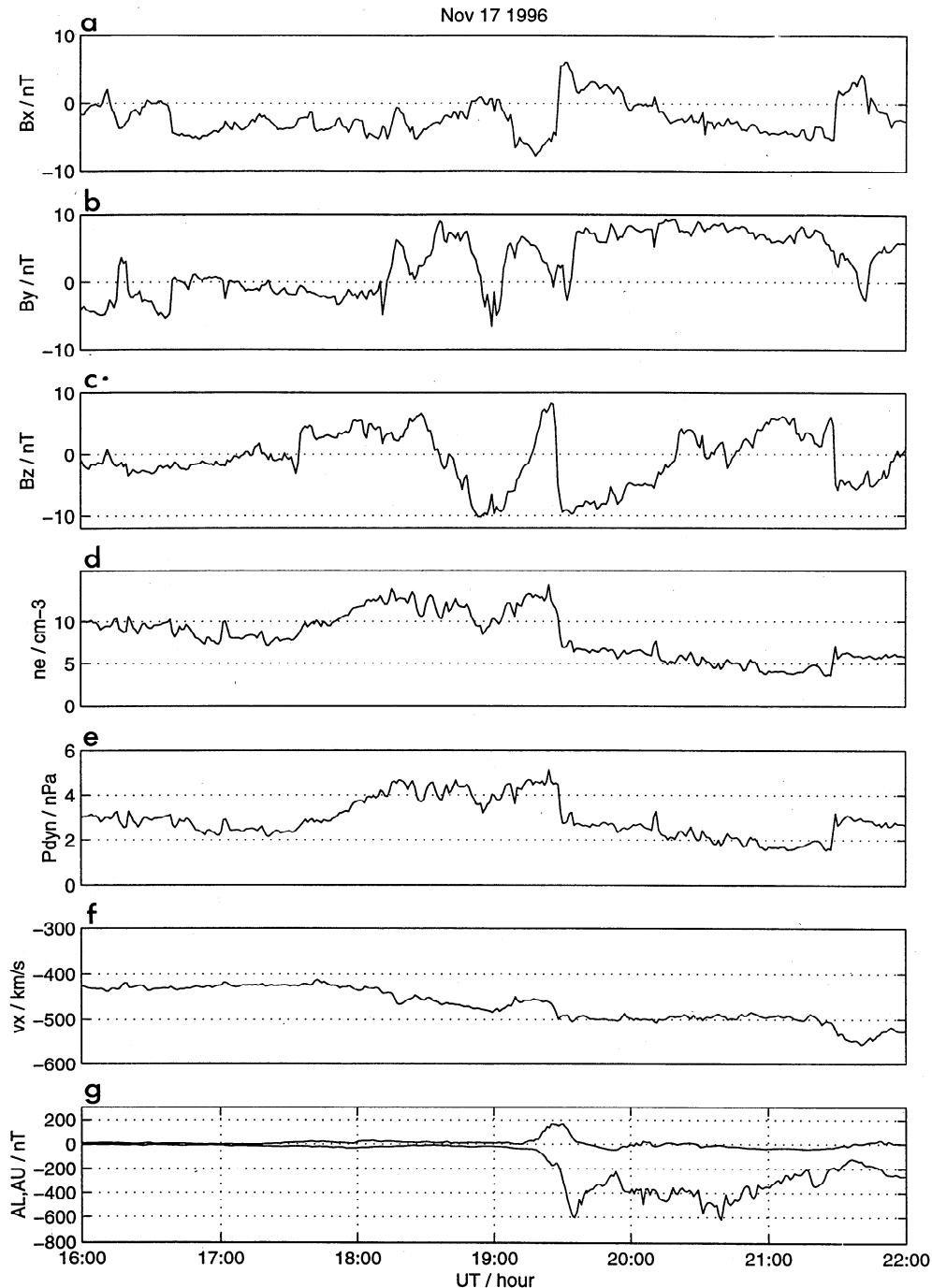


Figure 2. Solar wind observations on November 17, 1996, from the Wind satellite. (a-c) X , Y and Z components of the GSM interplanetary magnetic field, (d) Electron density, (e) Solar wind dynamic pressure, (f) X component of the solar wind velocity, and (g) for direct comparison the local auroral electrojet indices AL and AU , derived from the Scandinavian magnetometer network IMAGE (for maps see Figures 3a and Plate 2).

the sub-solar magnetopause, and Interball was in the northern magnetospheric lobe at $X = -26 R_E$ and $Z = 10 R_E$. We will show in section 2.2. that this constellation proved to be very favorable for the understanding of the event in question. Unfortunately, the IMP 8 satellite suffered from a data failure shortly before the sequence of events discussed here, so in Figure 2 we show the solar wind plasma data from the Wind space-

craft. Figures 2a-2c show from top to bottom the three magnetic vector components in the GSM co-ordinate system, Figures 2d-2f show the solar wind density, dynamic pressure and velocity, and in Figure 2g we display the local AL and AU indices as derived from the Scandinavian magnetometer network IMAGE. According to Kauristie *et al.* [1996] the local Auroral Electrojet (AE) index, derived from a single magnetometer

chain close to magnetic midnight, is a very good proxy for the real *AE* index. It can be seen that two southward turnings of the IMF at 1845 and 1928 UT are after some delay clearly associated with two substorm intensifications in the local *AE* index. While the second onset happens in a period of extended southward IMF, the first substorm occurs at a time when the solar wind undergoes changes in both the magnetic field and plasma pressure.

In section 2.1. we will first describe and discuss the individual observations made by the various ground-based instruments, in particular during and after the first of the two substorms. We will then provide a preliminary conclusion with a general description of the expected magnetospheric processes, which could account for the reported observations of ionospheric signatures. Then in section 2.2. we will in more detail inspect data from the Wind, Geotail, and Interball satellites in various regions of the solar wind-magnetosphere system, in order to verify our initial hypotheses from the ground-based data. Both data sets will be discussed together in section 3.

2.1. Ground-Based Observations

2.1.1. EISCAT. During the evening of November 17, 1996, the European Incoherent Scatter (EISCAT) facility [Folkestad *et al.*, 1983] was operated in a combined UHF Common Programme 1 (antenna pointing along B) and VHF Common Programme 7 mode (antenna pointing vertical). In the context of this paper we will concentrate on the UHF data on ionospheric plasma parameters plotted as a function of time and altitude shown in Plate 1. After a southward turning of the IMF at around 1845 UT (see Figure 2c), it can be seen that in Plate 1a (electron density) some minor auroral precipitation, giving enhanced electron densities near an altitude of about 120 km, becomes first visible at about 1850 UT and intensifies around 1900 UT, when a faint southward drifting growth phase arc enters the EISCAT UHF beam (for more details on other substorm growth phase signatures and auroral observations, see Figures 3a and 3b, Plate 2, and discussion below). The arc continues to drift toward south of the radar beam, leaving EISCAT to sound the area poleward of the auroral emissions; that is, the electron density is observed to decrease. After 1930 UT some very energetic precipitation suddenly reaches the EISCAT beam, resulting in ionization down to an altitude of 90–95 km. In section 2.1.2. we show that this precipitation is associated with a westward traveling surge (WTS) resulting from a storm onset at 1915 UT, initially located farther to the east of EISCAT. After the passage of the WTS, EISCAT records extremely low ionospheric ionization, even less than before the onset of growth phase signatures. It is interesting to note that this region of low ionization is associated with an intense ion heating event, illustrated in Plate 1c. Inspection of the total electric field measurements at an interception altitude of 275 km in

Plate 1d shows that this increase in the ion temperature is caused by strong ion frictional heating due to an intense electric field. The magnitude of this field (over 100 mV/m, corresponding to ion flow speeds of over 2 km/s) can be considered as high even in the vicinity of active auroral forms [Williams *et al.*, 1990]. The direction of the enhanced electric field inside the dark auroral region is south-southeast, and it was northward directed before the arrival of the first WTS (horizontal components not shown here). The strong electric fields lasted for about 20 min, until 1955 UT, when the WTS of a second substorm onset passes through the EISCAT UHF beam.

2.1.2. Optical and magnetic data. Figure 3a shows the development of the aurora and of the equivalent ionospheric current flow in the vicinity of EISCAT during the event. We have chosen typical and illustrative examples, overlaying the rectified image of a new digital Finnish all-sky camera in Muonio [Syrjäso, 1997] onto a map with horizontal equivalent current vectors, derived from the IMAGE network of magnetometers in Fenno-Scandinavia [Viljanen and Häkkinen, 1997]. The locations of the magnetometer stations are given in the first map of Figure 3a. The original temporal resolution is 10 s for the magnetometer data and 20 s for the optical data. Note that the spatial coverage of the original all-sky camera data (compare Figure 3b), in particular toward the off-diagonal directions, i.e., due north, south, east, and west, is much larger than the coordinate segment for which the images have been rectified for comparison with the magnetometer data in Figure 3a.

In the first map of Figure 3a at 1913 UT, a faint arc becomes visible, possibly being a weak intensification of a preexisting subvisual arc. At the same time the current system over the IMAGE network starts to develop faintly (compare also Plate 2). In map 1 of Figure 3a, the measured equivalent current vectors are still smaller than the symbols for the station location. The auroral arc moves southward (Figures 3a, Maps 2 and 3 at 1915 and 1917 UT, respectively), which is indicative of an ongoing substorm growth phase. As was shown in Figure 2c, a clear southward turning of the IMF was detected by the Wind satellite at 1845 UT, and the growth phase would be expected to begin when this southward turning reached the dayside magnetopause. Super Dual Auroral Radar Network (SuperDARN) data from Finland show at 1845 UT the start of a southward drift of a narrow region of F region backscatter, which was initially located at the poleward boundary of the auroral oval (data not shown here).

At 1915 UT, energetic particle measurements of the Los Alamos National Laboratory (LANL) geostationary satellite 1991-080 (Figure 5, see more detailed discussion in section 2.2.3) recorded an almost dispersionless injection of energetic electrons close to local magnetic midnight. Such injection features are considered as an unambiguous indicator of a nearby substorm onset. Lo-

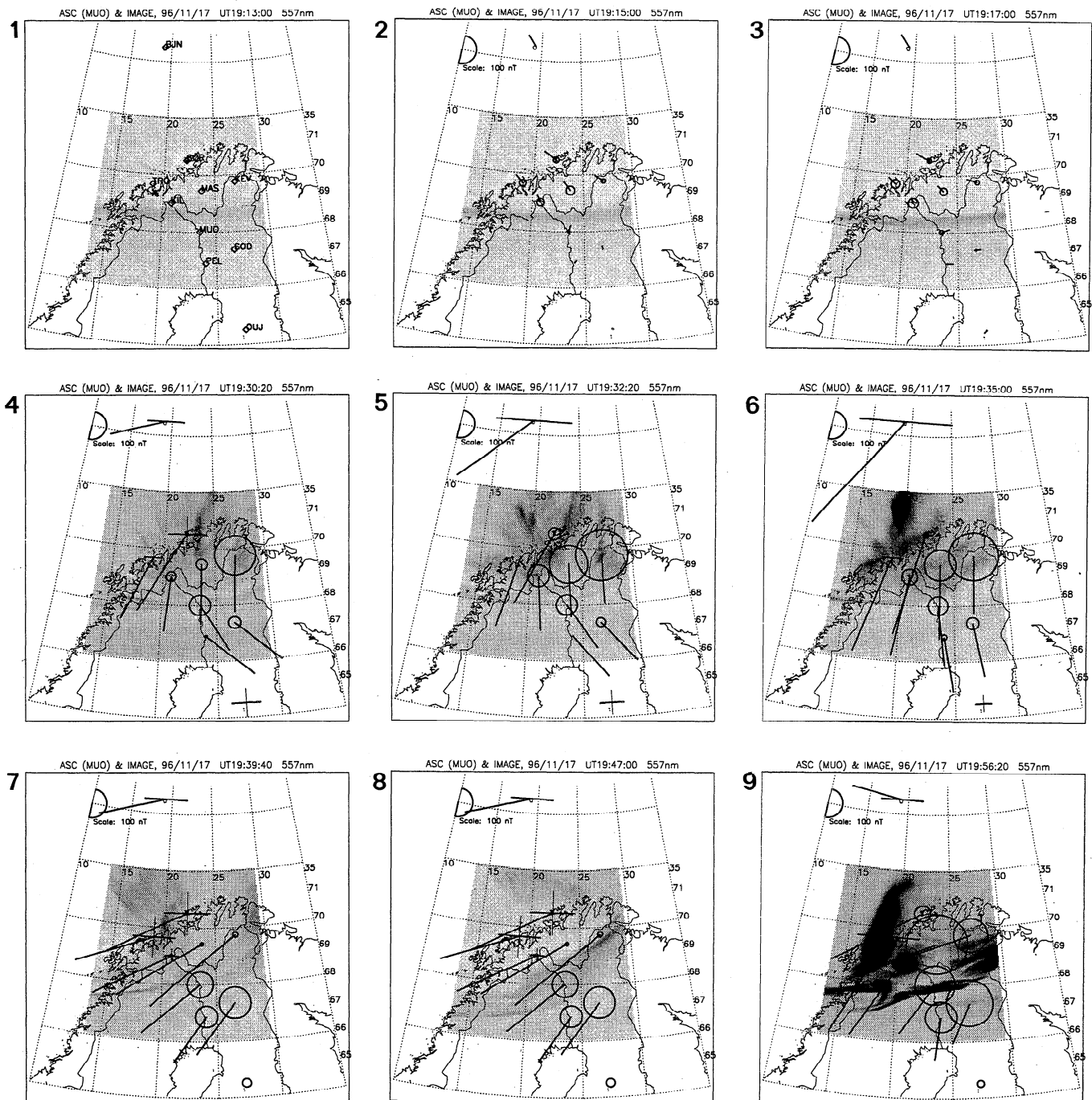


Figure 3a. Horizontal equivalent current vectors, derived from the central stations of the IMAGE magnetometer network, for selected time intervals during the passage of two westward traveling surges. The symbols at the footprint of the equivalent current vectors, circle and plus, demark the negative and positive deviations in the magnetic Z component, respectively, and the size of the symbol indicates the amplitude of the disturbance, in accordance to the scale in the top left corner. In map 1, at a time when the current vectors are still smaller than the station symbols, the station abbreviations are written next to each station location (KEV, Kevo; MAS, Maseide; KIL, Kilpisjärvi; MUO, Muonio; PEL, Pello; OIJ, Oulujärvi). At all instants the corresponding rectified auroral image of the Muonio all-sky camera is superimposed on the equivalent current vectors in order to allow for a direct comparison of current flow and precipitation regions.

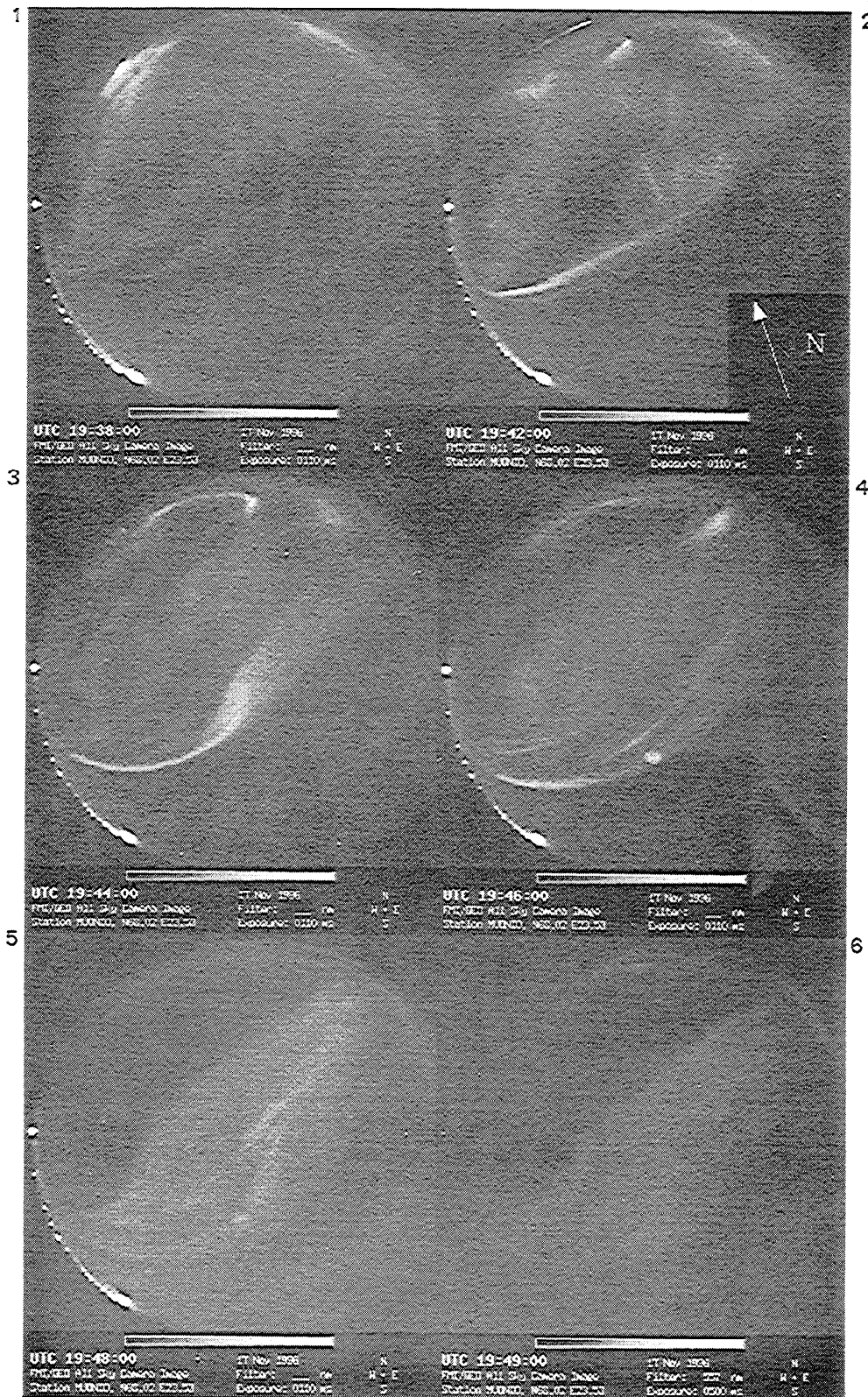


Figure 3b. Six selected frames of the original Muonio all-sky camera data for the period of the clearing of the poleward sky. Note that for the test operation during this particular night the camera was slightly rotated, so that the geographic north direction points about 17° to northwest (see arrow in bottom right corner of Frame 2).

cal magnetic midnight is at this moment located about 30° of longitude to the east of Fenno-Scandinavia. In fact, we see indications of this substorm onset already in the Scandinavian sector. In the original all-sky camera data (but not visible in the limited longitudinal coverage of the rectified image visible in Figure 3a, map 3), the very eastern sky clearly brightens just above the horizon at 1917 UT. Also the small eastward and westward electrojet systems, which grew very slowly throughout the substorm growth-phase, suddenly increase after 1915 UT (see also Plate 2a below). The auroral arc continues to drift southward until 1930 UT, when a westward traveling surge resulting from the substorm expansion reaches Scandinavia (Figure 3a, map 4), and creates the intense particle precipitation seen by EISCAT (Plate 1).

In Figure 3a, map 4, the equivalent current vectors in the vicinity of the surge form clearly show the typical pattern of a semicircular counterclockwise Hall current loop, containing an intense negative disturbance of the magnetic Z component. According to *Inhester et al.* [1981] and *Oppenoorth et al.* [1983], this equivalent ionospheric current pattern is indicative of a localized field-aligned current filament in the center of the optical surge. Map 5 then shows the continued westward propagation of the surge and the associated current pattern at 1932 UT, and in map 6, at 1935 UT, the western edge of the substorm expansion has left our field of view. However, already a few minutes later the aurora starts to fade from the north-west, and a region void of emissions is seen to expand toward southeast (Figure 3a, maps 7 and 8 at 1939 and 1947 UT, respectively).

As this development is not easily recognized in the selection of overview data in Figure 3a, we present the original all-sky camera data for this period in Figure 3b (note that the camera was slightly rotated during the night in question, so the geomagnetic north direction points about 17° to the left of the top of figure 3b, see arrow). In Frame 1 at 1938 UT the westward travelling surge has disappeared toward the west, and at this time the most poleward aurora starts to develop a small indentation, which grows within the following 10 min (Frames 2-6) into a large region void of emissions. The principal direction of the expansion of this dark region is south-southeast. By 1949 UT (Frame 6) the poleward sky has cleared from aurora, and no optical indications of the first substorm remain. From the magnetic disturbance data up to the latitude of Svalbard, shown in Plate 2, we can even exclude the possibility of a double auroral oval formation at this time, which would necessarily result in a second current maximum farther toward the north of Scandinavia. For the benefit of the discussion below we would also like to point out here that the aurora does not develop the typical diffuse, irregular, and patchy forms, which are normally seen after the passage of a WTS in the subsequent substorm recovery phase. In this case the remaining aurora is an equatorward drifting multiple auroral ar-

c, as is typically observed during the substorm growth phase.

However, in spite of the absence of auroral emissions in Figures 3a and 3b and, as indicated by the EISCAT data above, in the absence of virtually any ionizing precipitation, the equivalent current system continues to remain strong. For example, in Figure 3a, map 8, the peak of the westward current flow lies clearly to the north of the remaining auroral forms, inside the region devoid of aurora. It becomes obvious that the main agent for the current flow in this case is not enhanced conductivity inside the auroral precipitation region, as is normally observed for the DP1 substorm current, but instead a very intense electric field, as was observed by EISCAT (Plate 1).

It is interesting to note that the remaining auroral arc features after about 1940 UT drift southward in very much the same way as one would expect to see it drift in a substorm growth phase, and, indeed, at 1954 UT a new substorm bulge forms right over Scandinavia. The full development of this bulge is illustrated in Figure 3a, map 9 at 1956 UT. This second substorm onset, after first displaying the semicircular Hall current and Z component disturbance as is typically expected for the western edge of the expanding substorm current wedge, finally results in a broad and relatively stable westward substorm electrojet over the Scandinavian network of stations.

In order to clarify the development of the substorm electrojets, we display in Plate 2 the magnetic disturbances seen by the IMAGE magnetometer network in an alternative way. For the stations along the central meridian of the network (see maps in Figure 3a from Ny Alesund (NYA) to Oulujärvi (OUJ) and further extended by two more southerly stations Hankasalmi (HAN) and Nurmijärvi (NUR)) we calculated interpolated isocontours of the magnetic X , Y , and Z components versus latitude and time. In this presentation the enhancement of the large-scale eastward and westward electrojet shortly after the time of the substorm onset over Russia (1915 UT) becomes very pronounced (positive X disturbances at 64° latitude and negative at 70° latitude in Plate 2a). Also, the dramatic onsets of westward electrojet (increase of negative X component) and associated poleward expansion of the electrojet systems during the time of the two WTS passages at 1930 and 1955 UT are well recognized. An interesting feature in this presentation, which is not as apparent in other presentations of magnetic data, is the clear southward motion of the westward electrojet ($-X$ contours) after the first surge had decayed at 1940 UT (see above for a discussion of the southward motion of auroral forms during this time).

In Plate 2b the Y component iso-contours exhibit sharp positive disturbances associated with both observed surges, and in the Z component (Plate 2c) the step-like poleward expansions at both surge events become even more evident than in the X component in

EISCAT UHF Radar

CP1K November 17, 1996

Produced at IRF-U, 08-Mar-1999

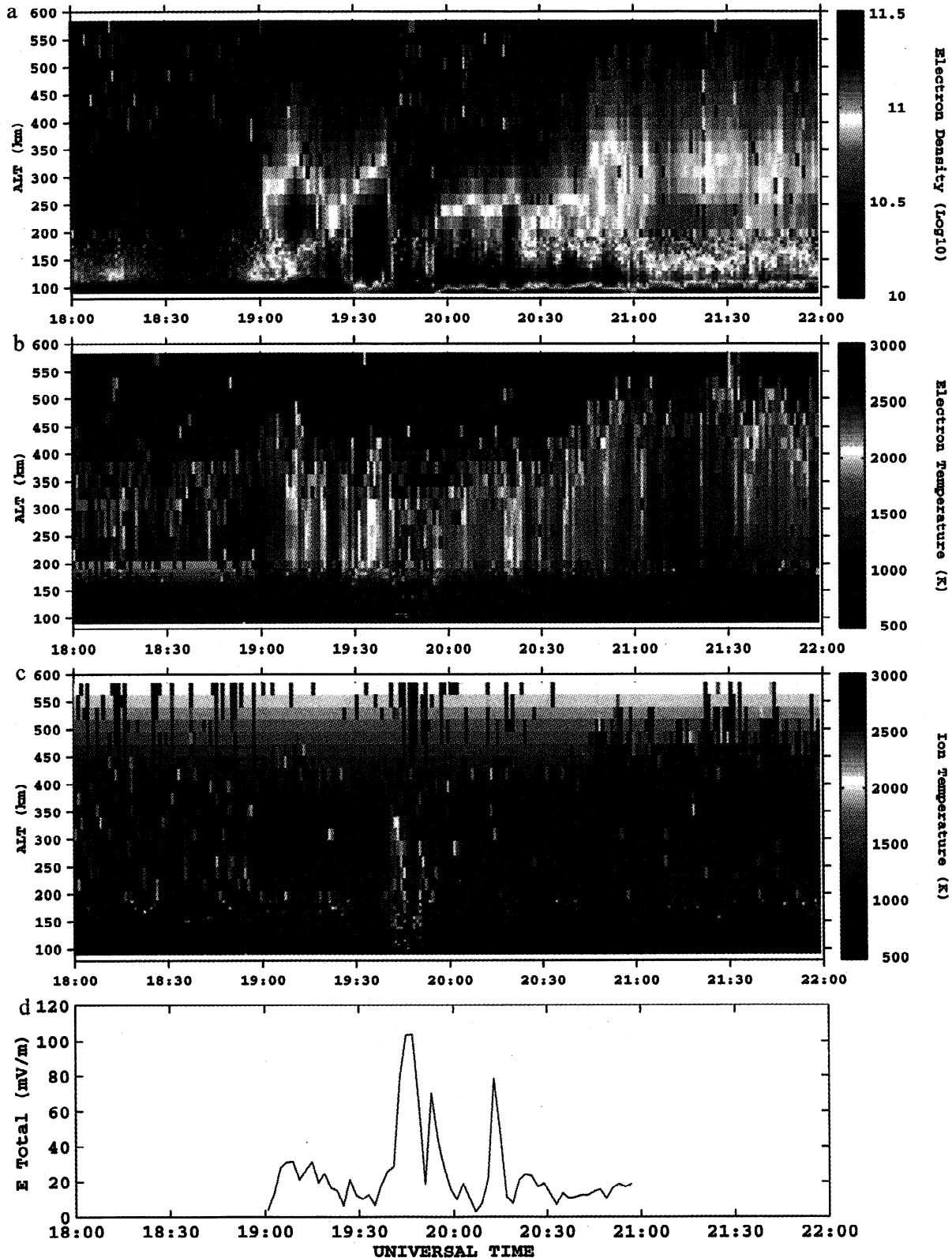


Plate 1. Ionospheric plasma parameters from 1800 to 2200 UT on November 17, 1996, as measured by the European Incoherent Scatter (EISCAT) UHF facility along the magnetic field line direction overhead Tromsø, Norway. (a) Electron density versus altitude and time. (b) Electron temperature versus altitude and time (c) Ion temperature versus altitude and time. (d) Total horizontal electric field component derived from the tristatic EISCAT remote station data at an altitude of 275 km.

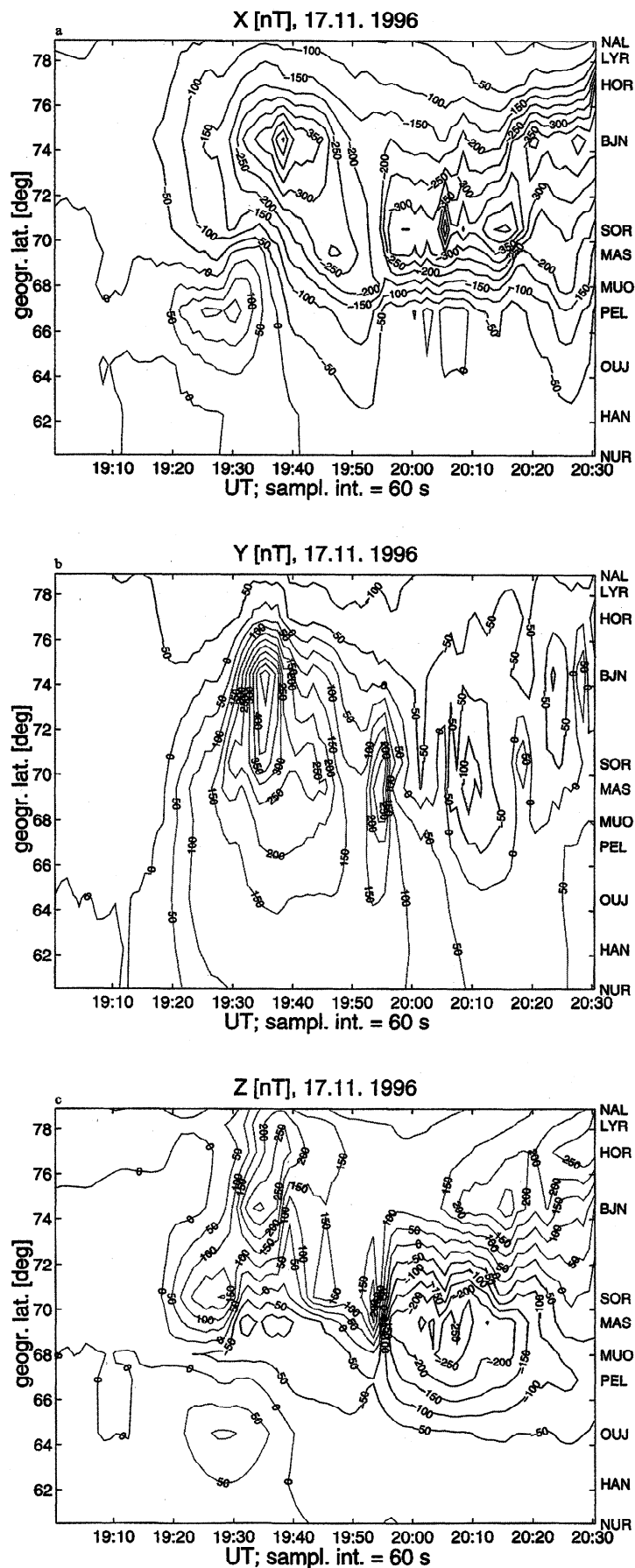


Plate 2. Positive, negative, and zero isocontour plots of magnetic component disturbances versus latitude and time along the central meridian of the IMAGE magnetometer network (see map in Figure 3a). (a) X component. (b) Y component. (c) Z component.

Plate 2a. Again, the southward drift of the Z component zero-contour line between 1935 and 1955 UT illustrates the growth phase like development between the two substorm expansions.

In summary, all the above observations combine into the following picture: a substorm onset, which is preceded by a typical growth phase, develops into a fairly large substorm expansion reaching about 75° in latitude, and we can follow its westward expansion for about 25° to 20° in longitude. However, for some reason the substorm does not continue to expand, and recovery-phase like features do not occur. Usually, after the maximum of the substorm expansion is reached, the recovery phase aurora is observed to fill the entire sky with irregular patchy forms. Flickering aurora often indicate resonances on the newly closed field-lines. Instead, in this case the northern sky clears again, and features very much resembling a renewed growth phase (with the exception of the remaining strong westward current in the dark auroral region) reoccur, i.e., southward drifting aurora, clearing of the poleward sky, and southward motion of electrojets. It appears as if the poleward portion of the previous auroral substorm bulge gets annihilated, but ionospheric currents continue to flow undiminished. Only the second substorm onset then develops into a stable westward electrojet, maximum auroral expansion, and typical irregular recovery phase feature after the full expansion was reached.

2.2. Satellite Observations

In sections 2.2.1 - 2.2.4 we will try to understand the reason for the relatively unusual behavior seen in the ground-based data which, to our knowledge, never before has been reported or at least has never explicitly been stressed. To this end we will inspect data from several ISTP satellites in various regions of the magnetosphere. As initially mentioned in section 2, this particular event was only recognized because of a specially arranged EISCAT experiment in coordination with a favorable ISTP satellite constellation.

2.2.1. Wind. It is not surprising that the dual growth phase behavior seen in the ground-based data sets is, in fact, closely associated with two periods of southward directed IMF from about 1845 to 1917 UT and from 1928 to beyond 2030 UT (see Wind data in Figure 2c). Only for a short period between 1917 and 1928 UT is the IMF direction northward. During this short northward excursion of the IMF the actual start of the decrease of southward IMF occurs already at about 1903 UT, simultaneously with a pronounced increase in the solar wind dynamic pressure, eventually reaching more than 5 nPa (see Figure 2e). A subsequent very sharp decrease of the solar wind pressure by about 2 nPa is seen in the Wind data at 1930 UT.

2.2.2. Geotail. In the Geotail data in Figure 4, recorded at $X = 11 R_E$, the most dramatic effect is caused by a clear compression of the magnetosphere between 1907 and 1920 UT, which must result from the

pressure pulse seen by Wind. Again, in Figure 4 we display magnetic field components, plasma density, dynamic pressure, and velocity but in this case not for the solar wind, but for the shocked magnetosheath plasma behind the bow shock, where Geotail is located for most of the time during the displayed period. One can recognize the two periods of southward directed magnetic field, now piled up to a much higher flux density, separated by a northward excursion between 1911 and 1922 UT. The pressure pulse becomes apparent in the Geotail data from the magnetosheath between about 1903 and 1924 UT.

The most interesting part of Figure 4 is, however, the period between 1907 and 1920 UT, when all curves undergo a jump in scale, indicating the satellite crossing of a clear boundary, which in this case must be the bow shock. From the solar wind data in Figure 2 and the magnetosheath data from Geotail in the closest vicinity of this bow shock crossing, it becomes evident that the observed pressure pulse with an amplitude of only about 2 nPa actually compresses the magnetosphere to such a degree that Geotail is passed by the compressed bow shock, finding itself on the outside, i.e., in the unshocked solar wind, for a duration of 13 min.

From a comparison of the relative timing between events seen by Wind and Geotail, we note that the onset of the pressure pulse and the initial decrease of southward IMF (the actual onset of a northward turning) occur almost simultaneously at the two satellites, while the exact zero crossing of the IMF B_z component and the rapid decay of the pressure pulse are observed with a delay of about 6 min between Geotail and Wind, in the somewhat unexpected sense that Wind observations are lagging behind Geotail observations in spite of their relative distance in X of almost $10 R_E$. This indicates that the solar wind shock fronts must have changed orientation within an interval of only 20 min. As this period is characterized by dramatic changes in both the IMF B_z and B_y components, such a behavior is not unlikely. Independent of eventual delays between Wind and Geotail, we conclude that the Geotail measurements are made very close to the subsolar magnetopause, and therefore must represent the exact impact times on the magnetosphere without further external delay. For example we have shown in section 2.1 that both periods of southward IMF lead within only a few minutes to clear growth phase features in the ground-based observations.

2.2.3. LANL geostationary satellite 1991-080.

In Figure 5 we show energetic electron observations of the LANL geostationary satellite 1991-080. During the time interval discussed in this paper satellite 1991-080 was located close to geomagnetic midnight over central Siberia. Two observations are of importance for the context of this paper. The first is, as mentioned in section 2.1.2, the almost dispersionless injection event at 1915 UT, indicating in accordance with other ground-based data the localized onset of a substorm about 20°

961117 GEOTAIL

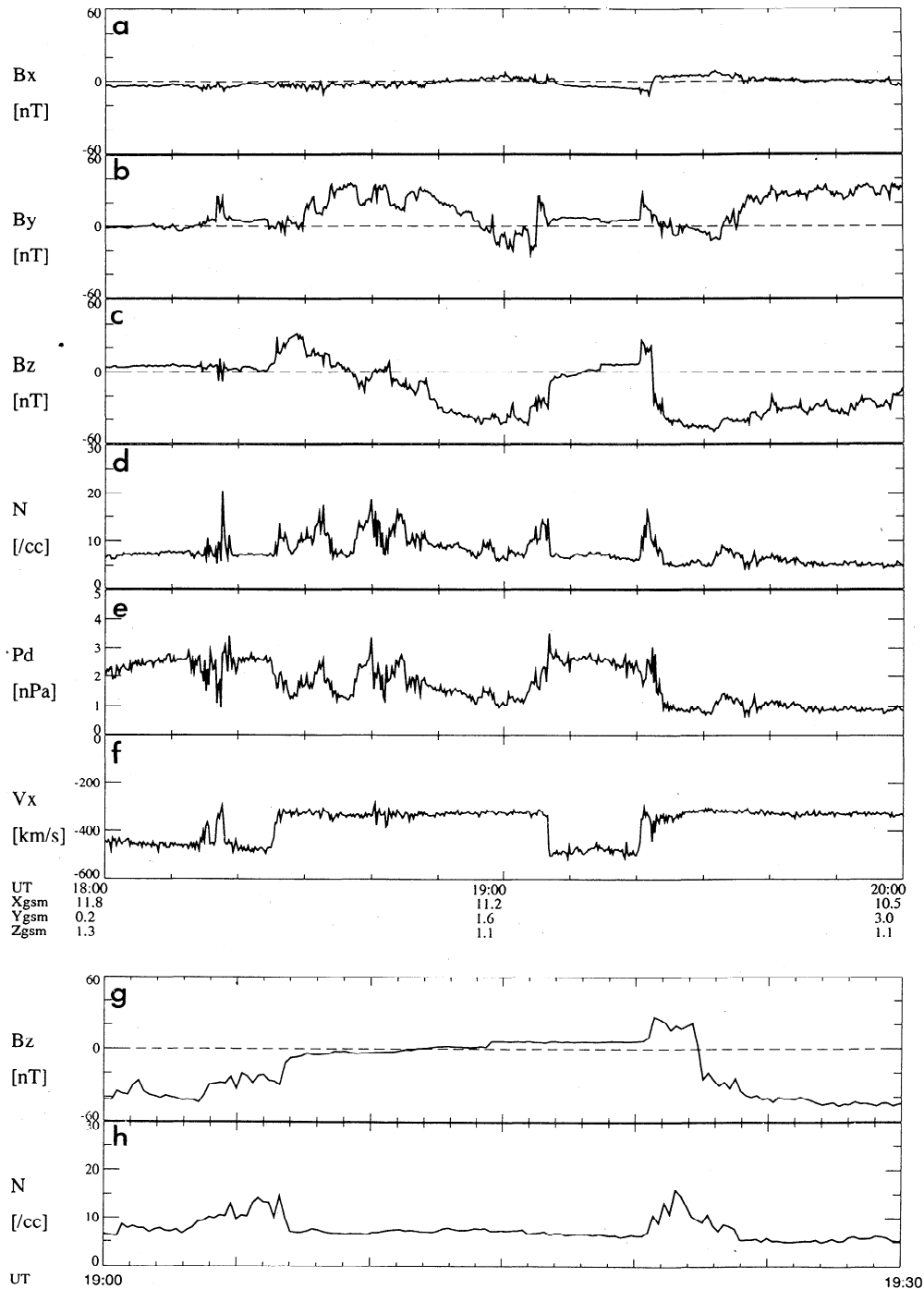


Figure 4. Multipanel plot of Geotail data just outside the subsolar magnetopause. (a-c) Interplanetary magnetic field components, (d) Electron density, (e) Dynamic pressure, (f) X component of the solar wind velocity. (g,h) Interplanetary magnetic field (IMF) B_z component and solar wind density on an expanded scale for the time period around the compression of the magnetosphere (see text).

- 30° east of Scandinavia, close to magnetic midnight. The second important observation in this data set is that the level of energetic electrons observed decreases very rapidly after injection, which is a rather uncommon behavior for substorm injections in a fully developed substorm.

Reeves *et al.* [1990] found that a typical injection signature at geosynchronous orbit lasts longer than one would expect if all particles were injected instantaneously over a limited region of space and then began their gradient curvature drift. They interpreted this as evidence that particles are continuously injected onto the

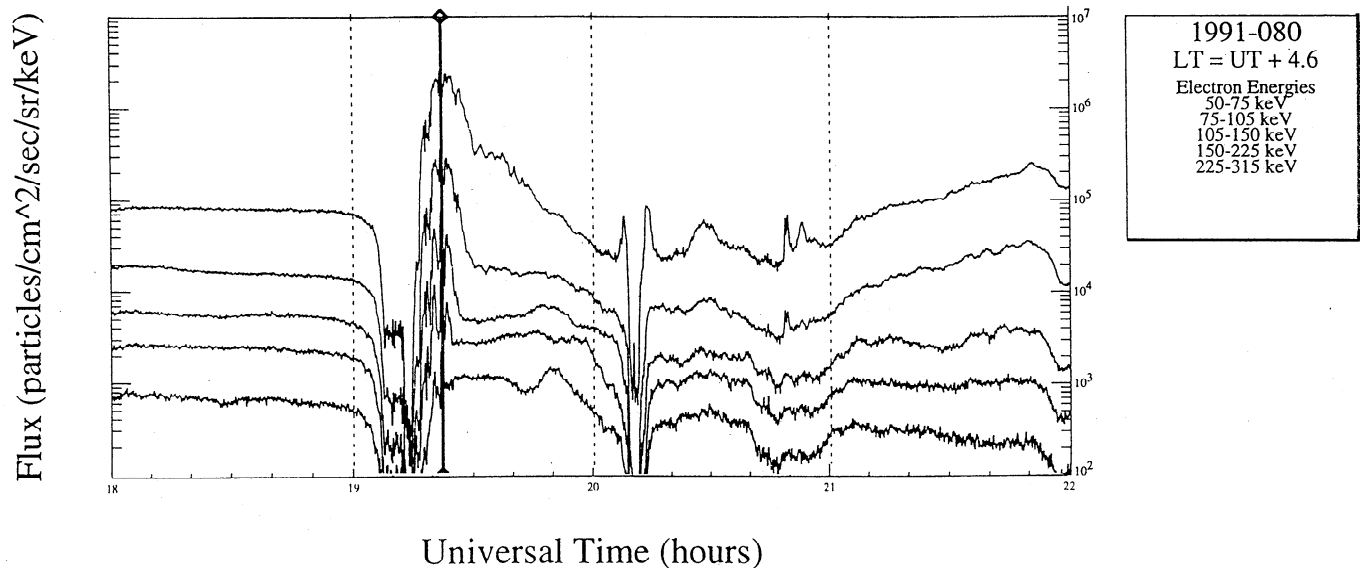


Figure 5. Substorm onset at 1915 UT as seen by the geostationary Los Alamos National Laboratory (LANL) satellite 1991-08 on November 17, 1996.

geosynchronous drift shell for a finite period of time and that the duration of the observed substorm injection feature is the sum of the finite duration of the substorm injection pulse plus the time required for injected particles to drift from the injection region past the satellite after the injection has stopped. The observations made in this case indicate that the mechanism, which continuously injected energetic substorm particles, was terminated shortly after 1927 UT. This is in agreement with the other observations of substorm termination in the ground-based data described in section 2.1. While it is known that the size of the injection region in local time extent can vary from event to event [e.g., *Reeves et al.*, 1992]) it is reasonable to expect that the signature of a quenched substorm would be an injection that was shorter in duration than a typical event and have a more rapid decrease of fluxes back to preinjection levels. Both signatures were observed in this event.

We also note that the second substorm onset, which was clearly observed in the ground-based data at 1956 UT, can at satellite 1991-080 only be identified in the most energetic particle channel. This indicates that in this case the bulk plasma distribution of the second injection does not penetrate to geostationary orbit, which at this time lies well within the previously dipolarized near-Earth magnetic fieldlines.

2.2.4. Interball. Finally, the magnetic field observations of Interball, located in the northern tail lobe at $X = -26 R_E$ and $Z = 10 R_E$, are displayed in Figure 6. In the following we will concentrate on the B_x -component, which in a first approximation of constant tail geometry is a proxy measure of the energy content of the magnetosphere but initially we would like to point out some interesting variations in the B_z component. Shortly after the substorm onset, timed by the ground-based network and the LANL satellite to

1915 UT, the B_z component grows initially more negative and then turns sharply into a positive direction, reaching positive values shortly after 1930 UT, before returning again to a lesser negative value. The whole feature of the temporal development in B_z resembles very much a superimposed bipolar structure, which has the right sense of sign as to be caused by the tailward passage of a Near-Earth Neutral Line (NENL) below the satellite, which must have formed earthward (in X) and below (in Z) of Interball's location. We will return to this observation in section 3.

Concerning the Interball observations of the lobe flux density B_l , which is basically represented by the B_x component, we are interested to evaluate how much of the observed change in B_x is caused by a change in the total open lobe flux F_T and how much change in B_x is related to compressions and expansions of the magnetosphere. Looking at the B_x component of Figure 6, it becomes obvious that the growth phase processes from about 1845 to 1915 UT lead to an increase in the lobe magnetic field of about 5 nT. At the moment of the first substorm onset at 1915 UT, B_x starts to decrease immediately, within the temporal resolution of the measurements. After 1930 UT it increases again during the second growth phase, just to decrease again after the second substorm onset at 1955 UT. On a first glance one would attribute these observed changes in the lobe flux density to actual production and destruction of open lobe flux in the substorm growth and expansion phase, respectively. Such a sudden and direct response of the lobe flux to substorm onset has earlier also been reported by *Fairfield and Lepping* [1981] and *McPherron et al.* [1993].

However, one must note a distinctly different feature in the rate of decrease of B_x after the first and second substorm onsets. As mentioned above, the second sub-

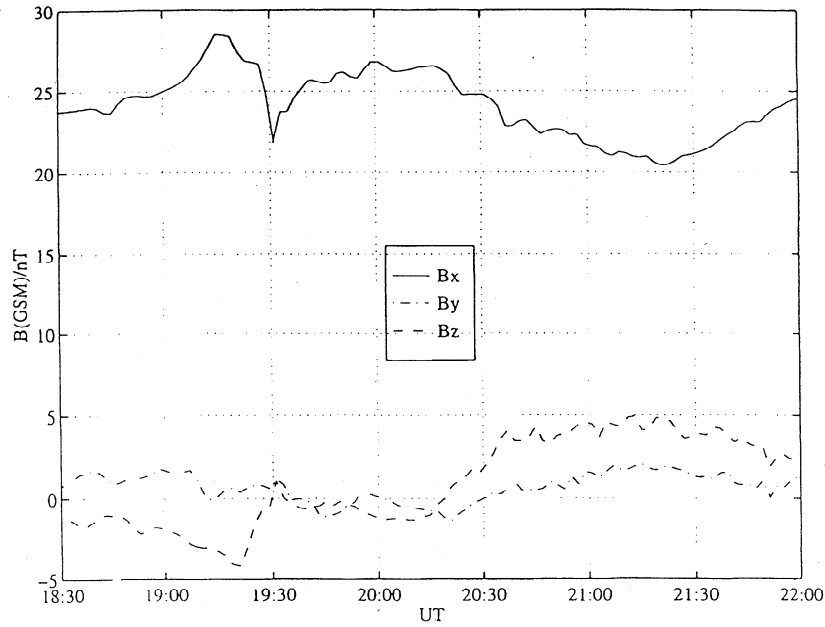


Figure 6. Interball magnetic field data from the northern tail lobe close to magnetic midnight at $X = -26 R_E$ and $Z = 10 R_E$ on November, 17, 1996.

storm expansion was more complete and also developed clear recovery phase features. Correspondingly, the observed decay of the lobe magnetic field after the second substorm is more extended and more gradual than that after the first one. A more detailed inspection of the data in Figure 6 for the first incomplete substorm reveals that the initial gradual decay of lobe magnetic field after substorm onset at 1915 UT abruptly changes into a much steeper decay between 1928 and 1930 UT. Not quite as obvious but still recognizable, there is also a change in the rate of the B_x increase shortly after 1900 UT. We note that these times are in accordance with the observation of dynamic pressure decrease and increase, respectively, at both Wind and Geotail. It is therefore more likely that these rapid effects are due to geometrical changes in the magnetosphere due to decompression and compression, respectively, caused by the observed variations in solar wind dynamic pressure.

In the following we want to investigate these rather speculative conclusions further. Using a relatively simple algorithm, we will estimate the effects of the solar wind pressure impact and release, resulting in compression and consequent relaxation of the magnetosphere, on the total lobe flux.

When the solar wind plasma impinges on the magnetopause, the bow shock converts bulk flow into higher temperatures and densities, and the thermal pressure becomes a significant term in the pressure balance condition; that is, the tail lobe pressure is balanced by both the dynamic pressure of the solar wind and its thermal pressure. In the so-called "Newtonian approximation" [Coroniti and Kennel, 1972] we find that

$$\frac{B_l^2}{2\mu_0} = P_{dyn} + P_{th} = N_{sw} m_i V_{sw}^2 \sin^2 \alpha + N_{sw} k (T_e + T_i), \quad (1)$$

where N_{sw} is the solar wind density, V_{sw} is the solar wind velocity, B_l is the tail lobe field strength and α is the magnetopause flaring angle. The ion mass of the solar wind can be assumed to be equal to 1.15 of the proton mass (i.e. a mixture of 95% protons and 5% Helium). This gives the following model expression for the tail lobe field strength:

$$B_l = \sqrt{2\mu_0 N_{sw} [k(T_e + T_i) + m_p V_{sw}^2 \sin^2 \alpha]}. \quad (2)$$

However, in this case we are interested not only in the calculation of the tail lobe magnetic field (as seen by Interball) on the basis of the solar wind parameters measured by Wind but also in the estimation of the total magnetospheric energy content, as represented by the total hemispheric polar cap flux F_T , which is an integral of B_l . To that end we consider, following the approach of Coroniti and Kennel [1972], the solar wind sonic Mach number $M = (P_{dyn}/P_{th})^{1/2}$, where P_{dyn} and P_{th} are the dynamic and thermal pressure terms in equation (1), respectively. At great distances the magnetospheric flaring angle α will go to zero, and thus, again using pressure balance, we can introduce an asymptotic tail radius $R_* = [F_T/(\mu_0 \pi^2 P_{th})]^{1/4}$, which provides the desired dependence on the total hemispheric flux F_T . Note that at these distances the shape of the magnetosphere is only determined by the thermal pressure as the magnetopause is aligned with the solar wind flow direction. Defining now a flaring tail scale length

$L = MR_0^3/3R_*^2$, where $R_0 = 15 R_E$ is a reference point radius at $x_0 = -5 R_E$, we can finally use the approximative equation (7) by Coroniti and Kennel, relating B_l to F_T :

$$B_l = \frac{2F_T}{\pi R_0^2} \times \left(1 + \frac{x_s - x_0}{L}\right)^{-2/3}. \quad (3)$$

However, we cannot use equations (1) - (3) right away to calculate F_T and α , because the theory of *Coroniti and Kennel* [1972] assumes homogeneous solar wind conditions or at least that the solar wind conditions do not vary along the range of X of the part of the tail that is considered. When the solar wind varies on short timescales (shorter than the travel time down the tail), this assumption will not be true. In order to arrive at a reasonable estimate of F_T and α , we therefore need to average out the smaller-scale fluctuations. In this case we consider the magnetosphere between the subsolar magnetopause at $X = 8 R_E$ and the location of the Interball satellite at $X = -26 R_E$. For the observed solar wind speed near 500 km/s at this time, this would require a travel time, and respectively an averaging period, of 7 min. In order to test this estimate, we used equation (2) and a constant flaring angle α to calculate B_l at Interball from the solar wind parameters measured by Wind, and we found the best agreement with the Interball B_x measurements at a time delay of 6 min. On the basis of these results, we finally averaged the wind data over the relevant 6 min periods and computed then the lobe flux F_l and the flaring angle α for each such period.

By Faraday's law, the rate of change of the lobe flux, dF/dt , is equal to the voltage difference dV . Because F_T is the flux threading a D-shaped Faraday loop made from where the cross tail and the magnetopause current sheets intersect the YZ plane at the X location of Interball, dV is the difference between the rate of antisunward transport of open flux to that plane and the rate of sunward transport of closed flux away from that plane. In effect, it is the reconnection voltage associated with open flux generation (but lagged by the transit time of that open flux from the magnetopause X-line to the X location of Interball), minus the reconnection voltage associated with the closure of open flux (but lagged by the transit time of that closed flux from the tail X-line to the X location of Interball). The derived variation in dV is inherently noisy as small fluctuations in the calculated F_T can cause very large and unphysical variations in dV on differentiating. Nevertheless, we found that the resulting gross variation was clear enough to reveal periods of positive dV , corresponding to growth phase accumulation of open flux at Interball, and negative dV , corresponding to expansion and recovery phase intervals in which the lobe flux at Interball is decreasing.

In Figure 7 we have finally plotted the results of such calculations for the solar wind flaring angle α at the X

location of Interball (Figure 7e), the total hemispheric flux F_T (Figure 7d) and the resulting voltage difference dV (Figure 7f) together with the solar wind thermal and dynamic pressure measured by Wind (Figure 7b and 7c) and the corresponding magnetic lobe pressure calculated from the original Interball lobe magnetic field measurement B_x (Figure 7a).

These data, inspected on the background of the other ground-based and satellite observations, allow for a number of valuable conclusions:

1. The first solar wind pressure enhancement seen by Wind between about 1805 and 1850 UT results in a decrease of the magnetospheric flaring angle α , as there is no previous growth phase effect added; the IMF direction is for most of this time strongly northward. Consequently, as already pointed out by, for example, *Petrinec and Russell* [1996], B_l does not vary very much. The dayside magnetospheric compression is fully compensated by a flaring of the tail. Also, no substorm activity is related to this period of enhanced solar wind pressure.

2. The second period of increased solar wind pressure falls into an advanced growth phase, about 25 min after Wind, IMP 8 and Geotail observe a southward turning of the IMF. Clear growth phase signatures are observed by all ground-based instruments. This time Interball observes at first a slow growth phase enhancement of B_l , followed at about 1905 UT by a strong reaction of B_l to the pressure enhancement. In this case it is interesting to note that the simultaneously observed northward turning of the IMF has a compensating effect on α , which remains more or less constant during the time interval of interest. Consequently, the effect of the magnetospheric compression enhances the already large B_l of the substorm growth phase. This combined effect of substorm growth phase and pressure pulse enhancement of the lobe field appears to be a very effective substorm trigger, as we observe the onset of the first substorm at 1915 UT.

3. It can be seen that the flaring angle α increases with southward IMF during both growth phases. A similar behavior of α was described by *Coroniti and Kennel* [1972] and furthermore expanded by *Petrinec and Russell* [1996]. However, we observe that in the case of the first substorm the expected increase in flaring angle is compensated by the solar wind pressure increase around 1900 UT. Nevertheless, the growth phase continues as seen in the continued growth of F_T (Figure 7d).

4. We note furthermore that the magnetic lobe pressure measured by Interball (Figure 7a) increases at that time more rapidly than the total flux, again in agreement with effects of the magnetospheric compression. After substorm onset at 1915 UT both the lobe magnetic field and the total flux decrease first gradually owing to plasma sheet collapse at the substorm onset, and at the time of magnetospheric relaxation, $P_{mag}(B_x)$ suddenly decreases more rapidly.

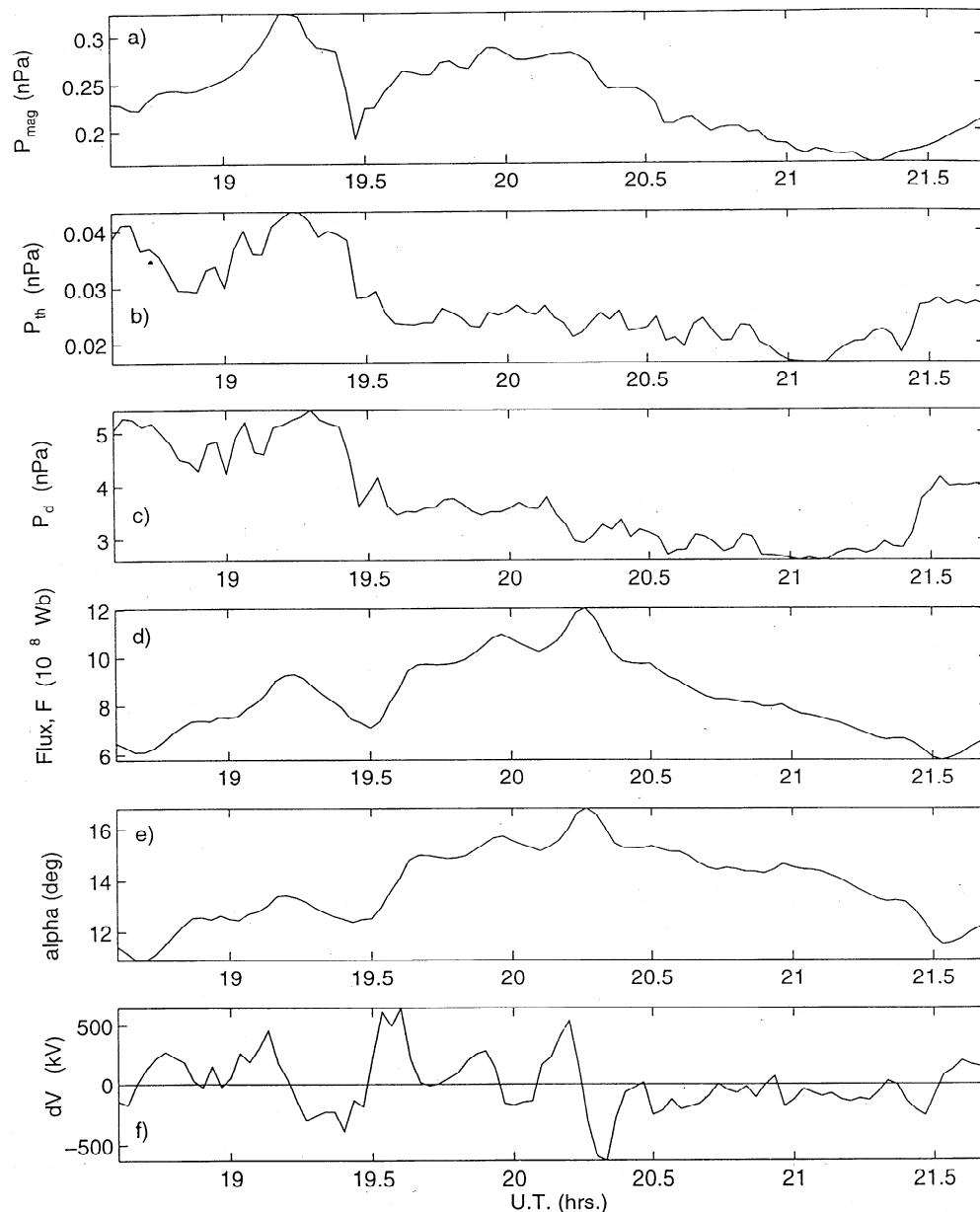


Figure 7. Magnetospheric plasma parameters derived from the Interball and Wind data presented in Figures 2 and 6 (see text for equations). (a) Magnetic lobe pressure, (b) Solar wind thermal pressure, (c) Solar wind dynamic pressure, (d) Hemispheric total open magnetic flux, (e) Magnetospheric flaring angle, (f) Rate of change of hemispheric open flux in terms of a voltage difference.

5. As concerns the total hemispheric magnetospheric open flux content (Figure 7d), we can identify two clear rises and falls in F_T , corresponding to two substorm cycles. The first cycle is shorter and of smaller amplitude than the second cycle. It is also much smaller than the observed variation in the lobe field. This is explained by the higher solar wind pressure at the time of this first substorm, which kept the tail more compressed. This effect is also reflected in the smaller values of α and the smaller amplitude of the variation in α . However, we note that it is the actual lobe flux density which controls the physics in the plasma sheet and the cross-tail cur-

rent. So the rapid rise and fall in lobe flux density are more likely the cause for the triggering and quenching of substorm onset.

6. The rate of change of open flux dV (displayed in Figure 7f) is variable but positive during the first substorm growth phase, and then it swings to negative near 1913 UT, very close to the observed time of substorm onset. Subsequently, it remains negative as lobe field is destroyed. This decline in open flux is not immediately altered by the arrival of the pressure drop, which causes the lobe field to decrease and the flaring angle to begin to increase, despite the fact that the lobe flux is still

decreasing. However, shortly thereafter, dV swings to strongly positive values, reflecting the renewed growth phase after the swing to southward IMF and probably a cessation of nightside reconnection as well. The subsequent rise in F_T in the growth phase of the second substorm is not smooth, giving rise to strong fluctuations in dV , which are similar to the variations in dV during the growth phase of the first substorm. These variations may either be due to some of the observed changes in the IMF B_z component or otherwise indicate some residual tail activity like, for example, bursty open flux destruction at a far X-line.

7. In addition, we note that the magnitude of dV is frequently greater than typical transpolar voltages seen in the ionosphere (up to an order of 150 kV). This is to be expected because rapid changes in the voltages contributing to dV will be inductively smoothed by the changes in the lobe field [Lockwood *et al.*, 1990].

3. Discussion

In this paper we have presented observational evidence of how a solar wind pressure pulse of only 2 nPa can compress and consequently release the magnetosphere to such a degree that the Geotail satellite, which was originally located in the magnetosheath, was passed by the bow shock and exited to the unshocked solar wind. We could also show that this magnetospheric compression and decompression had a clear effect on the magnetic flux density in the high-latitude magnetospheric lobes, as is seen by Interball. While it is not a particularly unexpected result that the solar wind dynamic pressure affects the magnetospheric topology and consequently also the lobe flux density, this particular event is interesting in so far that the short-lived magnetospheric deformation occurred within a well-developed substorm growth phase.

Observations from an extensive network of ground-based stations and a geostationary satellite showed that the pressure pulse was closely related to the onset (and consequent cessation) of a small magnetospheric substorm. We postulate that our observations indicate that the additional lobe flux density added by the solar wind pressure pulse was the responsible trigger agent to drive the, at that moment still stable, growth phase cross-tail current into an instability, causing initial substorm expansion. A comparable solar wind pressure enhancement, occurring just 1 hour before the event discussed here during a period of northward IMF, had no effect on magnetospheric substorm activity. A quite similar relation between the IMF direction (controlling the state of substorm growth phase) and the effectiveness of solar wind pressure increases on substorm activity was pointed out by *Petrinec and Russell* [1996]. They presented six case studies of SW pressure pulses, three of which were imbedded in southward IMF conditions and consequently were seen to trigger substorms. Three other examples occurred during periods of northward

IMF and therefore lead to no apparent ground magnetic disturbance in the auroral zone. *Shue and Kamide* [1998] recently presented another study in which they demonstrate how increased solar wind plasma density correlates well with substorm activity but only as long as IMF B_z is negative. *Jacquey* [1996] investigated the effect of changes in the IMF and solar wind plasma parameters on the lobe magnetic field B_l seen by the ISEE 1 satellite. In accordance with our observations he also noted that effective substorm triggering by solar wind pressure pulses only occurred during periods of already previously enhanced B_l .

Northward turnings of the IMF have long been advocated to play a role in substorm trigger [see, e.g., *Lyons*, 1995, 1996, and references therein], however, so far no obvious physical reason could be presented for why a decrease in energy loading should lead to a release of the already loaded energy, i.e., a substorm onset. Furthermore, a trigger mechanism based on IMF northward turnings is unable to account for the frequent substorm occurrence during periods of extended southward IMF (as presented in the above quoted works and in this paper for the second substorm). In this study we could also show that a strong northward turning occurred in very close temporal relation to the arrival of a SW pressure pulse and consequent substorm onset. We conclude that while one could easily point at the observed northward turning as a candidate for a substorm trigger, in our view of substorm energetics a sudden increase in lobe flux density, caused by a solar wind pressure increase, is still a much more likely trigger mechanism than the termination of the substorm growth phase by an IMF northward turning. While the former trigger has an immediate and positive effect on the plasma sheet current density (and thereby its stability), an IMF northward turn has only a slow and negative effect on the overall magnetospheric convection rate.

Pseudobreakups and so-called incomplete substorms are often discussed but seldom satisfactorily explained phenomena in substorm physics. Several authors, for example, *Nakamura et al.* [1994], *Pulkkinen* [1996], *Aikio et al.* [1996] and *Rostoker* [1998], have come to principally the same conclusion, namely, that pseudobreakups are caused by basically the same physical processes as complete substorms, resulting in similar features in the different magnetospheric and ionospheric plasma regimes. The only apparent difference is the temporal and spatial extent and the amount of energy released. Most papers dealing with pseudo-breakups leave one and the same question open: "What limits the release of energy after the pseudo-onset occurred?" We would like to point out that at least in the cases presented by *Aikio et al.* and *Rostoker* a quick check in the Coordinated Data Analysis Workshop (CDAW) internet database reveals that the sequence of pseudobreakups occurred in periods of extended southward directed IMF, and while there is no plasma data available

for the first case study, the event presented by Rostoker definitely contains a very variable solar wind pressure, with several clear pulses around the time of the multiple pseudobreakups. Also, in our case the initial substorms show all signs of a normal substorm: expansion of the auroral bulge, WTS, lobe field decrease, energetic particle injection, and even possibly the formation of a near-Earth neutral line inside of $X = -26 R_E$ (see Figure 6). Still, it was terminated before full expansion was reached, and no recovery occurred.

Therefore we find it interesting to discuss not only substorm onset but also the remarkable cessation of the first substorm presented here. Not unlike many other authors, even *Petrinec and Russell* [1996] only present the obvious substorm onset trigger effect by increases in the SW pressure. On the other hand, *Shue and Kamide* [1998] also point out that substorm activity decreases remarkably, when the solar wind pressure decreases, and that inspite of a continuously southward directed IMF. Above we have shown that after the initial substorm onset to the east of Scandinavia the ionospheric features expand as during any normal substorm, at least while the magnetosphere remains in a compressed state. However, as soon as the temporarily increased solar wind pressure is released, the lobe flux density is noticeably decreased to a far higher degree than is explainable by substorm reconnection (see Figures 6 and 7). We have shown furthermore that shortly after the effects of the magnetospheric decompression are monitored by Interball at $X = -26 R_E$, the substorm expansion stops and the expansion-phase aurora decreases and retreats from the very high latitudes toward a more normal oval location. Indications for a remarkably sudden substorm cessation were furthermore found in the geostationary satellite data of energetic electrons. The observed substorm injection was much shorter than normal, and the decrease to normal level was very rapid, starting at the same time as the other indications of substorm termination were seen in the ground-based data sets. Therefore we conclude that while these injection signatures by themselves do not prove the existence of substorm quenching in this event, they are consistent with that interpretation.

We interpret this overall and sudden disappearance of substorm activity (without clear recovery phase signatures) as caused by a "quenching" of the energy available for substorm expansion through a magnetospheric relaxation, caused by the sudden decrease in solar wind pressure. The resulting sudden decrease in lobe flux density as observed by Interball must be associated with a decrease of the cross-tail current, bringing it back to a subcritical and stable level. There exists no more reason for the just recently initiated instability to expand further tailward, and the ongoing substorm stops. Without any clear remainders of the previous substorm activity, the system goes back to new growth phase phenomena, driven and energized by a new southward turning of the IMF.

In this picture it is interesting to note where this quenching may have taken place. For this purpose we assume that the transportation of the compression/decompression through or rather along the magnetosphere happens with the velocity of the solar wind, transporting it alongside the magnetopause. In Figure 8 we sketch such a proposed geometry for the moment of substorm quenching, that is, when the relaxation has reached the X location of the tailward retreating near-Earth neutral line. Using the Wind measurements of the solar wind velocity (about 470 km/s on average during most of the interval of interest), the transport of the pressure release from the subsolar magnetopause to the location of Interball in the northern tail lobes at $X = -26 R_E$ should take about 7 min, we observe a 6 min delay as best fit between lobe flux variations calculated from Wind data and the actual Interball observations. In this estimate we do not consider any delay from the Wind location to the magnetopause, as we found no indication for that in the Geotail data from the subsolar magnetosheath. As we see the first indications for a decrease of the auroral activities at the northeasternmost edge of the field of view of our all-sky camera in Muonio at 1937 UT, we conclude that the decompression must have reached and affected the region for the still ongoing tailward substorm expansion just before that time, i.e., 1935-1936 UT. For this we consider a finite amount of time for the decreased precipitation to reach the ionosphere, and we also account for the possibility that the initial signatures of auroral decrease and cessation of substorm expansion may have started poleward of our field of view. In the data from the IMAGE magnetometer chain it is very clear that the substorm expansion reached as far poleward as Bear Island (BJN) at 1938 UT but immediately started to decay after reaching that latitude (see Plate 2a).

Considering 1935 - 1936 UT as the most probable time when the still expanding substorm mechanism was affected by the magnetospheric decompression, and noting that Interball measured drastically decreased lobe flux density at 1929 UT, we can put the region where the tailward progressing decompression must have affected the substorm process to about $X = -(26 + 30) = -56 \pm 5 R_E$. This is a quite reasonable distance for a tailward retreating NENL before reaching the distant neutral line, at about halfway through the substorm expansion. We can furthermore conclude that the observed disappearance of substorm aurora starting at the northern edge of the bulge (auroral retreat and clearing of the poleward sky) would be in agreement with a "recovery" of the plasma sheet from the tailward side inward (compare to Figure 8).

As presented above and earlier pointed out by *Fairfield and Lepping* [1981] and *McPherron et al.* [1993], the growth phase, as controlled by the southward component of the IMF, has a more or less direct effect on the magnetic flux density of the high-latitude magnetospheric lobes. The increase in lobe flux density accumu-

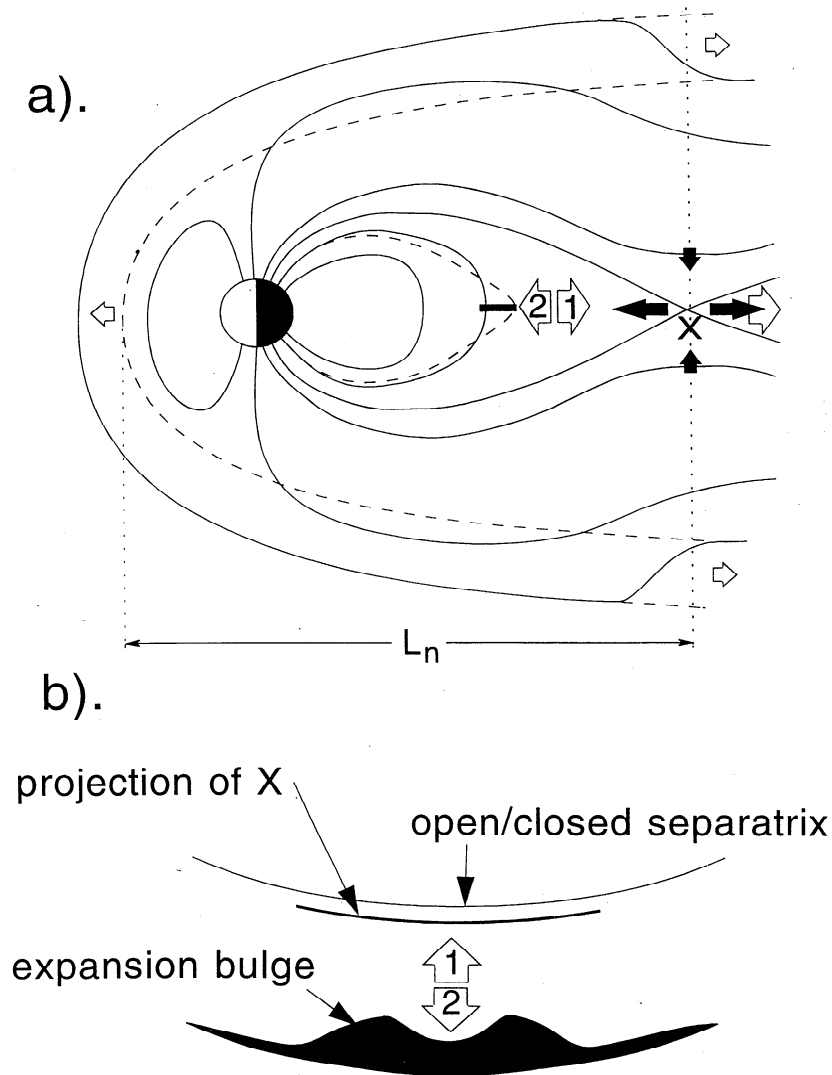


Figure 8. Illustration of how and where the expanding substorm instability could have been affected by a magnetospheric pressure release, carried along the flanks of the magnetosphere. (a) Sideview of the Near-Earth Neutral Line (NENL) model in the magnetospheric tail and (b) Ionospheric projection of the associated magnetospheric substorm expansion (1) and clearing of the poleward sky (2). See text for a more detailed discussion.

lated during the entire substorm growth phase is often, as is also in this paper, observed to decrease more or less immediately after substorm expansion onset. Both above quoted papers view this observation as an indicator for the existence of near-Earth magnetic flux destruction at a NENL. Such an immediate response in lobe flux is not easily predicted by the current disruption model, even though effects should be seen after a certain time interval, when the tailward expanding current disruption may have caused a NENL as a secondary effect [Lui, 1991, Kennel, 1992]. We see that in both substorm cases observed here the response in the lobe flux density to substorm onset is well marked and almost immediate to the accuracy of our measurements. In addition, we see, however, that compression and decompression of the magnetosphere can have an

even more pronounced effect, with much stronger temporal changes in B_l . Occurring at the right time (i.e., within a well developed but not yet completed substorm growth phase), it appears to be able to trigger the substorm instability and also reestablish a stable magnetospheric configuration.

A more thorough discussion of the possibility for quenching in the various substorm models is inappropriate for this first more observational paper. More details will be considered in a later paper, where we plan to investigate in what ways the here observed possibility of a quenched substorm expansion is accounted for in the various substorm models and whether our observations can be explained better by some models than others.

Besides the presented evidence that substorm quenching can occur in response to solar wind pressure vari-

ations, there are other interesting findings in this data set that deserve a further discussion. After the decrease and cessation of the first substorm we observe clear signatures that the magnetospheric convection has a considerable inertia. Once started up during the substorm onset and early expansion within the compressed magnetosphere, the increased convection cannot be annihilated as fast as the flux density in the lobes. The result of this is that the ionospheric currents remain relatively strong even after the substorm quenching. Around 1945 UT, i.e., when the magnetosphere already undergoes a renewed growth phase, the magnetometers still detect a relatively strong current flow in the region of the disappearing substorm aurora. Because of the fading of the substorm aurora and the disappearance of the associated conductivity enhancement, a strong ionospheric electric field is needed (and is observed by EISCAT).

This convection change is consistent with the concept of convection excitation proposed by Cowley and Lockwood [1992], allied to the effect of ionospheric conductivity changes, as is discussed by Morelli *et al.* [1993]. The distribution of potential around the open-closed field line boundary is set by the dayside and nightside reconnection voltages and their recent history. The flow streamlines driven by this voltage source in the closed field line region are also set by the spatial distribution of ionospheric conductivities. In substorm expansion it is difficult to establish field-aligned currents on the edge of the expansion region where conductivities suddenly rise. As a result, electric fields in that region drop so as to maintain a Pedersen current continuity across the boundaries. Conversely, on quenching the substorm the conductivities suddenly fall and the electric field rises to maintain the once excited current flow.

4. Summary and Conclusions

We have presented observations of an interesting substorm development, where a clear substorm onset and consecutive initial substorm expansion, covering several degrees in latitude and several tens of degrees in longitude, were abruptly terminated and did not develop any clear recovery phase signatures. Instead, the aurora withdrew from the poleward position, energetic particle precipitation to the ionosphere and injection to geostationary orbit stopped, and also the westward electrojet system retreated to more southern latitudes. Through careful analysis of data from several ISTP satellites in various regions of the magnetosphere, we could connect these observations with the effect of a solar wind pressure pulse of only 2 nPa, which initially compressed the magnetosphere to such a degree that substorm onset was triggered in an only partially completed growth phase. An earlier magnetospheric compression which occurred during a period of northward IMF, i.e., without previous energy loading, did not trigger substorm activity. Our observations furthermore strongly indicate that the following magnetospheric decompression

effectively quenched the energy available for continued substorm activity by a reduction of the lobe flux density and a corresponding decrease of the cross-tail current.

We conclude in agreement with Petrinec and Russell [1996] and Shue and Kamide [1998] that solar wind density variations during periods of southward IMF do play an important role in the occurrence of triggered substorms. Relatively short-lived solar wind pressure pulses might in particular be the reason for incomplete substorms, like, for example, so-called pseudobreakups, and series of multiple substorm onsets. While the changes in the IMF direction determine the total energy content of the magnetosphere via the total open lobe flux, short-lived variations of the solar wind pressure can have strong effects on the lobe field density. In the case of an already existing and slightly subcritical growth phase cross-tail current, as it would exist after some 30 min of continuous growth phase, solar wind induced lobe field density variations can strongly affect the stability or instability of the enhanced near-Earth cross-tail current.

Acknowledgments. The authors wish to thank the staff of EISCAT for their help in carrying out the experiment. The EISCAT Scientific Association is supported by the SA of Finland, CNRS of France, MPG of Germany, NFR of Norway, NFR of Sweden, PPARC of the United Kingdom, and NIPR of Japan. We would like to thank A. Huuskonen for providing us with EISCAT electric field data and P. Janhunen for interesting discussions on ionospheric reaction to solar wind forcing. We also thank R. P. Lepping for Wind plasma data (received via ISTP WWW pages) and T. Mukai for Geotail particle data. We finally acknowledge Ari Viljanen for maintenance of the IMAGE magnetometer chain. S. B. P. Karlsson and P. Eglitis acknowledge support from NFR. Parts of H. J. Opgenoorth's work were carried out during a visiting professorship at STELAB, Toyokawa, Japan.

Michel Blanc thanks Christopher Russell and another referee for their assistance in evaluating this paper.

References

- Aikio, A., V. Sergeev, M. Shukhtina, L. Vagina, and G. Reeves, Case study of a sequence of substorms, in *Proceedings of the Third International Conference on Substorms, Versailles, France, 12-17 May 1996*, Eur. Space Agency, Spec. Publ. ESA SP-389, 315-320, 1996.
- Baker, D. N., E. W. Hones, Jr., D. T. Young, and J. Birn, The possible role of ionospheric oxygen in the initiation and development of plasma sheet instabilities, *Geophys. Res. Lett.*, **9**, 1337, 1982.
- Baker, D. N., S.-I. Akasofu, W. Baumjohann, J. W. Bieber, D. H. Fairfield, E. W. Hones, Jr., B. H. Mauk, R. L. McPherron, and T. E. Moore, Substorms in the magnetosphere, in *Solar Terrestrial Physics: Present and Future*, chap. 8, NASA Ref. Publ., 1120, 1984.
- Baker, D. N., T. A. Fritz, R. L. McPherron, D. H. Fairfield, Y. Kamide, and W. Baumjohann, Magnetotail energy storage and release during the CDaw 6 substorm analysis intervals, *J. Geophys. Res.*, **90**, 1205, 1985.
- Baker, D. N., T. I. Pulkkinen, V. Angelopoulos, W. Baumjohann, and R. L. McPherron, Neutral line model of substorms: Past results and present view, *J. Geophys. Res.*, **101**, 12,975, 1996.

- Caan, M. N., R. L. McPherron, and C. T. Russell, Solar wind and substorm-related changes in the lobes of the geomagnetic tail, *J. Geophys. Res.*, **78**, 8087, 1973.
- Coroniti, F. V., and C. F. Kennel, Changes in magnetospheric configuration in the substorm growth phase, *J. Geophys. Res.*, **77**, 3361, 1972.
- Cowley, S. W. H., and M. Lockwood, Excitation and decay of solar wind-driven flows in the magnetosphere-ionosphere system, *Ann. Geophys.*, **10**, 103, 1992.
- Daglis, I. A., and W. I. Axford, Fast ionospheric response to enhanced activity in geospace: Ion feeding of the inner magnetotail, *J. Geophys. Res.*, **101**, 5047, 1996.
- Daglis, I. A., S. Livi, E. T. Sarris, and B. Wilken, Energy density of ionospheric and solar wind origin ions in the near-Earth magnetotail during substorms, *J. Geophys. Res.*, **99**, 5691, 1994.
- Eastman, T. E., L. A. Frank, and C. Y. Huang, The boundary layers as the primary transport regions of the Earth's magnetotail, *J. Geophys. Res.*, **90**, 9541, 1985.
- Eastman, T. E., G. Rostoker, L. A. Frank, C. Y. Huang, and D. G. Mitchell, Boundary layer dynamics in the description of magnetospheric substorms, *J. Geophys. Res.*, **93**, 14,411, 1988.
- Elphinstone, R. D., J. S. Murphree, and L. L. Cogger, What is a global auroral substorm? *Rev. Geophys.*, **34**, 169, 1996.
- Fairfield, D. H., and R. P. Lepping, Simultaneous measurements of magnetotail dynamics by IMP spacecraft, *J. Geophys. Res.*, **86**, 1396, 1981.
- Folkestad, K., T. Hagfors, and S. Westerlund, EISCAT: an updated description of technical characteristics and operational capabilities, *Radio Sci.*, **18**, 867, 1983.
- Hesse, M., and J. Birn, Magnetosphere-ionosphere coupling during plasmoid evolution: First results, *J. Geophys. Res.*, **96**, 11,513, 1991a.
- Hesse, M., and J. Birn, On dipolarization and its relationship to the substorm current wedge, *J. Geophys. Res.*, **96**, 19,417, 1991b.
- Hones, E. W., Jr., C. D. Anger, J. Birn, J. S. Murphree, and L. L. Cogger, A study of a magnetospheric substorm recorded by the Viking auroral imager, *Geophys. Res. Lett.*, **14**, 411, 1987.
- Inhester, B., W. Baumjohann, R. A. Greenwald, and E. Nielsen, Joint two-dimensional observations of ground magnetic and ionospheric electric fields associated with auroral zone currents: 3. Auroral zone currents during the passage of a westward traveling surge, *J. Geophys.*, **49**, 155, 1981.
- Jacquey, C., Time-variation of the large scale tail magnetic field prior substorm related to solar wind changes, in *Proceedings of the Third International Conference on Substorms, Versailles, France, 12-17 May 1996, Europ. Space Agency Spec. Publ. ESA SP-389*, 295-300, 1996.
- Kan, J. R., A global magnetosphere-ionosphere coupling model of substorms, *J. Geophys. Res.*, **98**, 17,263, 1993.
- Kauristie, K., T. I. Pulkkinen, R. J. Pellinen, and H. J. Opgenoorth, What can we tell about global auroral electrojet activity from a single meridional magnetometer chain?, *Ann. Geophys.*, **14**, 1177, 1996.
- Kennel, C., The Kiruna conjecture: The strong version, in *Proceedings of the International Conference on Substorms (ICS-1), Kiruna, Sweden, March 1992, Europ. Space Agency Spec. Publ., ESA SP-335*, 599, 1992.
- Koskinen, H. E. J., T. I. Pulkkinen, R. J. Pellinen, T. Bösinger, D. N. Baker, and R. E. Lopez, Characteristics of pseudobreakups, in *Proceedings of the International Conference on Substorms (ICS-1), Kiruna, Sweden, March 1992, Europ. Space Agency Spec. Publ., ESA SP-335*, 111, 1992.
- Lockwood, M., S. W. H. Cowley, and M. P. Freeman, The excitation of plasma convection in the high latitude ionosphere, *J. Geophys. Res.*, **95**, 7961, 1990.
- Lopez, R. E., and A. T. Y. Lui, A multisatellite case study of the expansion of a substorm current wedge in the near-Earth magnetotail, *J. Geophys. Res.*, **95**, 8009, 1990.
- Lopez, R., A. T. Y. Lui, D. G. Sibeck, R. W. McEntire, L. J. Zanetti, T. A. Potemra, and S. M. Krimigis, The longitudinal and radial distribution of magnetic reconfigurations in the near-Earth magnetotail as observed by AMPTE CCE, *J. Geophys. Res.*, **93**, 997, 1988.
- Lui, A. T. Y., A synthesis of magnetospheric substorm models, *J. Geophys. Res.*, **96**, 1849, 1991.
- Lui, A. T. Y., R. E. Lopez, B. J. Anderson, K. Takahashi, L. J. Zanetti, R. W. McEntire, T. A. Potemra, D. M. Klumpar, E. M. Greene, and R. Strangeway, Current disruptions in the near-Earth neutral sheet region, *J. Geophys. Res.*, **97**, 1461, 1992.
- Lyons, L. R., A new theory for magnetospheric substorms, *J. Geophys. Res.*, **100**, 19,069, 1995.
- Lyons, L. R., Substorms: Fundamental observational features, distinction from other disturbances, and external triggering, *J. Geophys. Res.*, **101**, 13,011, 1996.
- McPherron, R. L., Growth pPhase of magnetospheric substorms, *J. Geophys. Res.*, **75**, 5592, 1970.
- McPherron, R. L., Substorm related changes in the geomagnetic tail: The growth phase, *Planet. Space Sci.*, **20**, 1521, 1972.
- McPherron, R. L., Physical processes producing magnetospheric substorms and magnetic storms, *Geomagnetism*, **4**, 593, 1991.
- McPherron, R. L., C. T. Russell, and M. P. Aubry, Satellite studies of magnetospheric substorms on August 15, 1968, 9, Phenomenological model for substorms, *J. Geophys. Res.*, **78**, 3131, 1973.
- McPherron, R. L., V. Angelopoulos, D. N. Baker, and E. W. Hones, Jr., Is there a near-Earth neutral line?, *Adv. Space Res.*, **13**, (4), 173, 1993.
- Morelli, J. P., et al., Plasma flow bursts in the nightside auroral zone ionosphere and their relation to geomagnetic activity, *Adv. Space Res.*, **13**, (4), 135, 1993.
- Nakamura, R., D. N. Baker, T. Yamamoto, R. D. Belian, E. A. Bering III, J. R. Benbrook, and J. R. Theall, Particle and field signatures during pseudobreakup and major expansion onset, *J. Geophys. Res.*, **99**, 207, 1994.
- Opgenoorth, H. J., R. J. Pellinen, W. Baumjohann, E. Nielsen, G. Marklund, and L. Eliasson, Three-dimensional current flow and particle precipitation in a westward travelling surge (Observed during the Barium-Geos rocket experiment), *J. Geophys. Res.*, **88**, 3138, 1983.
- Opgenoorth, H. J., M. A. L. Persson, T. I. Pulkkinen, and R. J. Pellinen, The recovery phase of magnetospheric substorms and its association with morning-sector aurora, *J. Geophys. Res.*, **99**, 4115, 1994.
- Pellinen, R. J., H. J. Opgenoorth, and T. I. Pulkkinen, Substorm recovery phase: Relationship to next activation, in *Proceedings of the International Conference on Substorms (ICS-1), Kiruna, Sweden, March 1992, Eur. Space Agency Spec. Publ., ESA SP-335*, 469, 1992.
- Petrinec, S. M. and C. T. Russell, Near-Earth magnetotail shape and size as determined from the magnetopause flaring angle, *J. Geophys. Res.*, **101**, 137, 1996.
- Pulkkinen, T. I., Pseudobreakup or substorm?, in *Proceedings of the Third International Conference on Substorms, Versailles, France, 12-17 May 1996, Eur. Space Agency Spec. Publ., ESA SP-389*, 285, 1996.
- Reeves, G. D., T. A. Fritz, T. E. Cayton, and R. D. Belian,

- Multi-satellite measurements of the substorm injection region, *Geophys. Res. Lett.*, **17**, 2015, 1990.
- Reeves, G. D., G. Kettmann, T. A. Fritz, and R. D. Belian, Further investigation of the CDAW 7 substorm using geosynchronous particle data: Multiple injections and their implications, *J. Geophys. Res.*, **97**, 6417, 1992.
- Rostoker, G., Triggering of expansive phase intensifications of magnetospheric substorms by northward turnings of the interplanetary magnetic field, *J. Geophys. Res.*, **88**, 6981, 1983.
- Rostoker, G., Phenomenology and physics of magnetospheric substorms, *J. Geophys. Res.*, **101**, 12973, 1996.
- Rostoker, G., On the place of the pseudo-breakup in a magnetospheric substorm, *Geophys. Res. Lett.*, **25**, 217, 1998.
- Russell, C. T., and R. L. McPherron, The magnetotail and substorms, *Space Sci. Rev.*, **15**, 205, 1973.
- Sergeev, V. A., R. J. Pellinen, and T. I. Pulkkinen, Steady magnetospheric convection: A review of recent results, *Space Sci. Rev.*, **75**, 551, 1996.
- Shue, J.-H., and Y. Kamide, Effects of solar wind density on the westward electrojet, in *Proceedings of the Fourth International Conference on Substorms, Lake Hamana, Japan, 9-13 March 1998*, 667, Terra Sci., Tokyo, Japan, 1998.
- Syrjäso, M., New Finnish All-Sky Cameras, Paper presented at the 24th Optical Meeting, Andenes, Norway, August, 1997.
- Viljanen, A., and L. Häkkinen, IMAGE magnetometer network, in *Satellite Ground-Based Coordination Sourcebook, Eur. Space Agency Spec. Publ., ESA-SP1198*, 111, 1997.
- Williams, D. J., D. G. Mitchell, C. Y. Huang, L. A. Frank, and C. T. Russell, Particle acceleration during substorm growth and onset, *Geophys. Res. Lett.*, **17**, 587, 1990.
- Yeoman, T. K., H. Lühr, R. W. H. Friedel, S. Coles, M. Grande, C. H. Perry, M. Lester, P. N. Smith, H. J. Singer, and D. Orr, CRRES/ground-based multi-instrument observations of an interval of substorm activity, *Ann. Geophys.*, **12**, 1158, 1994.

P. Eglitis, S. B. P. Karlsson, and H. J. Opgenoorth, Swedish Institute of Space Physics, Uppsala Division, S-79551 Uppsala, Sweden. (opg@irfu.se)

K. Kauristie, T. Pulkkinen, and M. Syrjäso, Finnish Meteorological Institute, Box 503, FIN-00101 Helsinki, Finland.

M. Lockwood, Rutherford Appleton Laboratory, Chilton, Didcot, Oxfordshire, OX11 0QX, England, UK.

R. Nakamura, Max-Planck-Institut für Extraterrestrische Physik, Postfach 1603, D-84740 Garching, Germany.

G. Reeves, Los Alamos National Laboratory, Los Alamos, NM 87545.

S. Romanov, Space Research Institute, Russian Academy of Sciences, Profsoyuznaya str. 84/31, Moscow 117810, Russia.

(Received April 20, 1998; revised June 4, 1999; accepted June 17, 1999.)